Quantum networking with photons and trapped atoms (Invited)

D. L. Moehring, M. J. Madsen, K. C. Younge, R. N. Kohn, Jr., P. Maunz, L.-M. Duan, and C. Monroe

FOCUS Center and Department of Physics, University of Michigan, Ann Arbor, Michigan 48109-1040

B. B. Blinov

Department of Physics, University of Washington, Seattle, Washington 98195

Received June 21, 2006; accepted July 14, 2006;
posted August 15, 2006 (Doc. ID 72166); published January 26, 2007

Distributed quantum information processing requires a reliable quantum memory and a faithful carrier of quantum information. Atomic qubits have very long coherence times and are thus excellent candidates for quantum information storage, whereas photons are ideal for the transport of quantum information as they can travel long distances with a minimum of decoherence. We discuss the theoretical and experimental combination of these two systems and their use for not only quantum information transfer but also scalable quantum computation architectures.

OCIS codes: 020.7010, 270.5580, 020.1670, 270.5290.

1. INTRODUCTION

Trapped atoms are among the most attractive systems for scalable quantum computation as they can be well isolated from the environment and manipulated easily with lasers.[1–22] However, as one tries to scale these systems to many hundreds or thousands of atomic quantum bits (qubits), current experimental setups may be too limited to deal with the complexity of these very large systems. One approach to overcome this scaling problem in ion traps is to shuttle the ions through multizone traps.[23–26] In such a system, quantum gates are performed in entangling zones of the larger trap structure, and the atoms are shuttled to other zones for storage or further operations as necessary. Still, as the number of atoms grows and the dimensions of the traps shrink, preserving coherence may become exceedingly difficult.[27]

Another approach to scaling up atomic quantum computation systems is to use photon-mediated entanglement. With this approach, atoms in many different trapping zones can be entangled without the need for cooling to the motional ground state or even localization within the Lamb–Dicke regime. Even though this approach is typically probabilistic, it has been shown to scale polynomially with $1/P_{\mathrm{a-a}}$ and n ($P_{\mathrm{a-a}}$ is the success probability for atom–atom entanglement in a given trial, and n is the number of qubits),[28–30] thus eliminating the need for challenging cavity-QED techniques necessary for the generation of deterministic quantum information transfer between atomic and photonic sources.[13,14,22,31] While QED techniques are not strictly necessary, they can be incorporated into the protocols described in this paper and can help to increase the probability of spontaneously emitting a photon into the mode of interest.

Probabilistic atom entanglement leads to deterministic quantum computation in a way similar to linear optical quantum computing where quantum interference of two photons is used to create quantum gates. By combining atomic and photonic systems, the benefits of atomic quantum memory[32–34] and the quantum communication of photons are combined. If two photons emitted by two atomic sources interfere on a beam splitter (BS), then the appropriate measurement of the photons from the two atoms can project the atoms into an entangled state that can be used as a resource for further quantum information processing.

Here, we present a theoretical and experimental overview of the entanglement between atomic and photonic systems. We show the progress toward the generation of probabilistic remote atom entanglement, and how this entanglement provides a key component for scalable quantum computation. Although work with trapped atomic ions is highlighted in this paper, all the techniques discussed are also applicable to neutral atoms and perhaps even isolated quantum dots.[35–39]

This paper starts with a general introduction to the entanglement between a single atom and a single photon. Next, we show how remote entanglement can be created using atom–photon entangled pairs and is followed by experimental progress toward this end. The paper concludes with a discussion on how this approach to remote-atom entanglement, though probabilistic, can lead to scalable quantum computation.

2. PROBABILISTIC ENTANGLEMENT BETWEEN A SINGLE ATOM AND A SINGLE PHOTON

Consider an atomic system possessing long-lived electronic states that can be used as a viable qubit and also having a strong electric dipole coupling to an excited electronic state. For concreteness, the atomic qubit states are assumed to be hyperfine levels in the $^2S_{1/2}$ ground states

0740-3224/07/020300-16/$15.00

of a single valence electron atom,[40] although other atomic level schemes can be used. We assume the atomic system has short-lived $^2P_{1/2}$ and $^2P_{3/2}$ excited states that spontaneously decay exclusively to the $^2S_{1/2}$ ground state. Similar systems with decay channels to other electronic states (such as low-lying ^2D states) may also apply but require the application of radiation driving population from these states back to the $S-P$ levels.

When a single atom is prepared in one of the excited ^2P states, a single photon can be spontaneously emitted via multiple decay channels after a mean time of τ (the natural lifetime of the P state) typically in the nanosecond range. Attributes of the emitted photon from the multiple decay channels can become entangled with the resulting $^2S_{1/2}$ ground states of the atom.

The simplest atomic level diagram for this system (nuclear spin $I=1/2$) is shown in Fig. 1(a). The main requirement for atom–photon entanglement is to drive the atom to a state with multiple decay channels, which result in different levels of the atomic ground state $|S_i\rangle$. The resulting (unnormalized) state of the photon and atom is

$$\Psi = \sum_{i,j,\Delta m} C_{i,j,\Delta m}|S_i\rangle|\nu_j\rangle|\Pi_{\Delta m}\rangle, \tag{1}$$

where $C_{i,j,\Delta m}$ are atomic Clebsch–Gordon (CG) coefficients, ν_j are the photon frequencies, and $\Pi_{\Delta m}$ are the photon polarizations.

The photons are emitted in a specific radiation pattern depending on the change in angular momentum of the atom along the quantization axis, Δm (defined by an applied magnetic field of typically a few Gauss [Fig. 1(g)]). For $\Delta m=0$, the (unnormalized) polarization state of a spontaneously emitted photon is $|\Pi_0\rangle=-\sin\theta|\hat{\theta}\rangle$ and for $\Delta m=\pm 1$, the states are $|\Pi_{\pm 1}\rangle=e^{\pm i\phi}(\cos\theta|\hat{\theta}\rangle\pm i|\hat{\phi}\rangle)/\sqrt{2}$, where θ and ϕ are spherical polar and azimuthal angles of the emitted photon's wave vector with respect to the quantization axis, and $\hat{\theta}$ and $\hat{\phi}$ are their associated spherical coordinate unit vectors. Based on these formulas, there are a number of protocols, which are good candidates for atom–photon entanglement, five of which are illustrated in Figs. 1(b)–1(f).

Ideally, the atom will decay to two different $^2S_{1/2}$ levels via two distinct decay channels of distinguishable photon qubit states (either polarization or frequency states). Polarization qubits typically require the photon to be emitted in a specific direction. One convenient choice is for a photon emitted perpendicularly to the dipole axis ($\theta=\pi/2$). In this case, the $\Delta m=\pm 1$ radiation is linearly polarized and orthogonal to the $\Delta m=0$ radiation. Another possibility is emission along the quantization axis ($\theta=0$). Here, no $\Delta m=0$ photons are emitted due to the radiation intensity pattern [Fig. 1(g)]; whereas the $\Delta m=\pm 1$ photons have opposite (orthogonal) helicity. With polarization qubits, single-qubit rotations are easily accomplished via quarter- and half-wave plates, and qubit state detection is done with polarizing BSs and single-photon detectors.

One possible decay scheme is shown in Fig. 1(b), where the $^2P_{3/2}$ $|2,1\rangle$ state is prepared. From here, the atom spontaneously decays back to either the $^2S_{1/2}$ $|1,0\rangle$ ($|\downarrow\rangle$) state while emitting a σ^+-polarized photon or to the $^2S_{1/2}$ $|1,1\rangle$ ($|\uparrow\rangle$) state while emitting a π-polarized photon (with identical CG coefficients). With this decay scheme, the photon polarizations are orthogonal when viewed perpendicularly to the quantization axis, with the π decay photon polarized parallel to the quantization axis (defined as $|V\rangle$), and the σ^+ decay photon polarized perpendicularly to the quantization axis (defined as $|H\rangle$). The resulting atom–photon entangled state is $\sqrt{1/3}|\downarrow\rangle|H\rangle+\sqrt{2/3}|\uparrow\rangle|V\rangle$, where the different prefactors come from the spatial radiation intensity modes for $\Delta m=-1$ and $\Delta m=0$ transitions. Although this state is not a maximally entangled Bell state, it is still sufficient for multiatom entanglement experiments as shown later.

Figures 1(c) and 1(d) show similar decay schemes, which give rise to entanglement between the atomic qubit

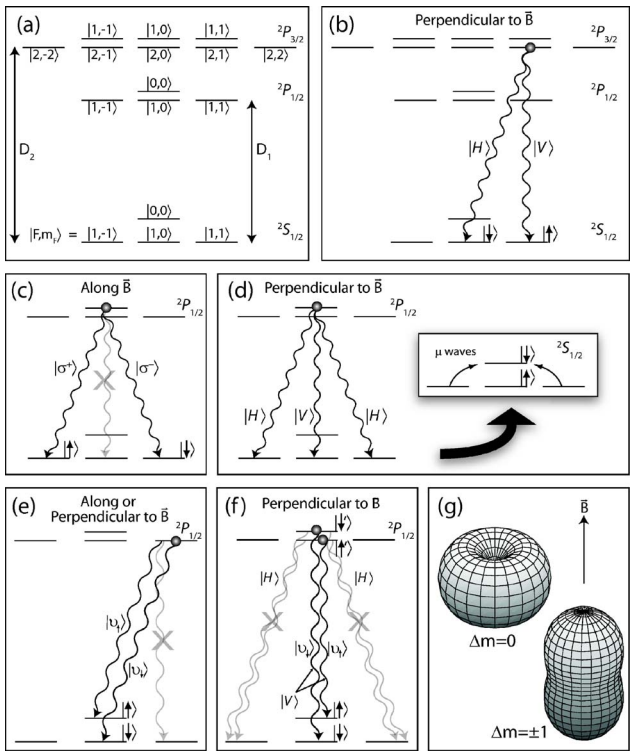

Fig. 1. Possible schemes for atom–photon entanglement. (a) Energy level diagram for an atom with nuclear spin $I=1/2$ and magnetic moment $\mu_I<0$. (b) Decay scheme unique to the $^2P_{3/2}$ level with two possible decay channels. If the photon is emitted perpendicularly to the quantization axis, the polarization modes are linear and orthogonal. (c) Decay scheme consisting of three decay channels where viewing along the quantization axis eliminates the photon from the $\Delta m=0$ decay channel due to the radiation pattern, and the $\Delta m=\pm 1$ photons have orthogonal circular polarizations. (d) Same decay scheme as (c) but viewed perpendicularly to the quantization axis. The $\Delta m=0$ photon decay channel is linear and orthogonal to the $\Delta m=\pm 1$ decay channels. After decay, the $|1,-1\rangle$ and $|1,1\rangle$ can be coherently combined in the $|0,0\rangle$ state establishing the atomic qubit. (e) Two $|\Delta m|=1$ decay channels with the same polarization comprise a photonic frequency qubit. The $\Delta m=0$ photon can be eliminated by a polarizer or by the radiation pattern if viewed along the quantization axis. (f) Two $\Delta m=0$ decay channels with the same polarization and different frequencies. Viewed perpendicularly to the quantization axis, the $\Delta m=\pm 1$ photons are eliminated via a polarizer. As described in the text, this decay scheme can be used to perform quantum gates between the atom and the photon. [Note that cases (c)–(f) also apply to the $^2P_{3/2}$ levels.] (g) Radiation emission patterns for the $\Delta m=0$ and $\Delta m=\pm 1$ decay channels defined by a magnetic field $\vec{B}$.

and the photon polarization qubit. In both of these schemes, the atom is prepared in the $^2P_{1/2}$ $|0,0\rangle$ (or $^2P_{3/2}$ $|2, 0\rangle$) state with three decay channels. Along the quantization axis [Fig. 1(c)], no $\Delta m=0$ photons are detected due to the radiation pattern, and the $\Delta m=\pm 1$ photons have orthogonal circular polarizations. The resulting polarizations can be converted into the $|H\rangle-|V\rangle$ basis with a quarter-wave plate creating the $(|\downarrow\rangle|H\rangle+|\uparrow\rangle|V\rangle)/\sqrt{2}$ Bell state. Similarly, if observed perpendicularly to the quantization axis [Fig. 1(d)], the polarization of the $\Delta m=0$ decay channel is orthogonal to the $\Delta m=\pm 1$ decay channels. While this results in populating three atomic levels, $|1, -1\rangle$ and $|1,1\rangle$ can be coherently combined in the $|0,0\rangle$ state transferring the population to the clock qubit states.[40]

In addition to photon polarizations, two resolved frequencies can also be used for the photonic qubit. As compared with polarization qubits, frequency qubits can be difficult to manipulate, as it is much more challenging to separate and detect frequency components (typically separated by a few gigahertz for atomic systems) than to measure different polarization modes. However, direct measurement of the photon frequency qubits is possible by using a Mach–Zehnder interferometer with a path length difference equal to $c/2\Delta\nu$, where $\Delta\nu$ is the frequency splitting of the photonic qubit. Qubit rotations can also be performed by changing the path length difference of the interferometer. One technical challenge for further atomic state rotations is synchronization of the photon arrival time with the free evolution of the atomic hyperfine qubit ($1/\Delta\nu=100$ ps for $\Delta\nu=10$ GHz), which may be feasible using very fast electronics and detectors. However, direct diagnosis of the photonic qubit is not necessary when performing remote-atom entanglement, as will be shown later.

With remote entanglement, frequency qubits are expected to be more robust than polarization qubits. Closely spaced frequency components of the same polarization have essentially zero dispersion in typical optical paths and thus are highly insensitive to phase jitter and birefringence inherent in optical paths.[41–47] Furthermore, because these frequency qubit states have the same spatial emission patterns, efficient mode matching is possible even with an increased collection solid angle.[30]

One scheme using frequency qubits is shown in Fig. 1(e), where an atom prepared in the $^2P_{1/2}$ $|1,1\rangle$ state decays to the $^2S_{1/2}$ $|1,0\rangle$ and $|0,0\rangle$ states emitting a photon with a single polarization but in a superposition of different frequencies. Here, a π-polarized photon to the $^2S_{1/2}$ $|1,1\rangle$ state can be eliminated via a polarizer or by detecting along the quantization axis resulting in the atom–photon entangled state $(|\uparrow\rangle|\nu_\uparrow\rangle+|\downarrow\rangle|\nu_\downarrow\rangle)/\sqrt{2}$.

While either photonic qubit allows for the creation of entanglement between atoms and photons, frequency qubits further enable the possibility to propagate prior superposition or entanglement of the atom to the photon, which can be used for quantum gates.[30] Consider the setup illustrated in Fig. 1(f), where an atom (of half-integer I) is initially prepared in a superposition of the magnetic field insensitive clock qubit states $|F,m_F=0\rangle \equiv|\uparrow\rangle$, and $|F+1,m_F=0\rangle\equiv|\downarrow\rangle$. Upon excitation with a π-polarized laser pulse, the atom can be coherently driven to the corresponding clock qubit states in the excited $^2P_{1/2}$ levels,[48,49] $|F'+1,m_{F'}=0\rangle\equiv|\uparrow'\rangle$, and $|F',m_{F'}=0\rangle\equiv|\downarrow'\rangle$ respectively, where $F'=F$. Cross coupling between the levels $|\uparrow\rangle\leftrightarrow|\downarrow'\rangle$ and $|\downarrow\rangle\leftrightarrow|\uparrow'\rangle$ is prohibited by selection rules. After spontaneous emission of a π-polarized photon into the appropriate mode (with $\Delta m=\pm 1$ photons eliminated via a polarizer), the atom and photon are entangled in the state $c_\uparrow|\uparrow\rangle|\nu_\uparrow\rangle+c_\downarrow|\downarrow\rangle|\nu_\downarrow\rangle$, where $c_\uparrow$ and $c_\downarrow$ correspond to the initial superposition amplitudes of the atom before excitation.

For any of the atom–photon entanglement schemes described above, the probability of detecting the entanglement in a given trial is less than unity, $P_{\text{a–p}}\equiv p_e p<1$. Here, p_e is the probability of single photon emission (atomic excitation), and $p=f\eta T(\Delta\Omega/4\pi)$ is the probability of a photon being detected in the desired spatial mode, where $f=I_{\Delta\Omega}/\langle I\rangle$ is of order unity and describes the intensity of the atomic emission pattern into the light collection solid angle $\Delta\Omega$ compared to the average emission intensity over all space, η is the quantum efficiency of the single-photon detectors, and T is the optical transmission. This results in an atom–photon entanglement success rate of $R_{\text{a–p}}=P_{\text{a–p}}/T_{\text{rep}}$, where the repetition time T_{rep} can be of the order of the excited state lifetime, τ.

Ideally, $P_{\text{a–p}}$ could approach unity. The excitation probability could be near unity by using an ultrafast laser pulse ($p_e\sim 1$) as discussed in more detail later. One could also increase the collection efficiency of scattered photons by placing the atom within an optical cavity. This could potentially allow for the collection of all scattered photons, effectively allowing $\Delta\Omega/4\pi$ to approach unity without sacrificing fidelity.[17,22,50,51] Photon detector efficiencies can also be near perfect.[52–54] Nonetheless, the success probability on a given trial is assumed in the following discussions to be $p\ll 1$.

3. ENTANGLING TWO ATOMIC QUBITS THROUGH INTERFERENCE OF PHOTONS

Atoms separated by a distance too large for significant atom–atom interactions may instead be entangled via their emitted photons. Protocols that accomplish this require the ability to mode match photons produced by two atoms such that, after a BS, the photons from each atom are indistinguishable.[55–57]

In one such protocol, proposed by Cabrillo *et al.*,[55] two atoms are each prepared in a known ground state $|\downarrow\rangle$ of a three-level λ system [Fig. 2(a)]. The two atoms are then simultaneously weakly driven ($p_e=\epsilon\ll 1$) to the excited state $|e\rangle$ from where the atom will decay either to the original state or to a second ground state $|\uparrow\rangle$. After the weak excitation pulse, the two atoms are each in the (unnormalized) state $|\downarrow\rangle+\sqrt{\epsilon}|e\rangle$ or for atoms a and b: $(|\downarrow\rangle_a+\sqrt{\epsilon}|e\rangle_a)\otimes(|\downarrow\rangle_b+\sqrt{\epsilon}|e\rangle_b)=|\downarrow\rangle_a|\downarrow\rangle_b+\sqrt{\epsilon}|\downarrow\rangle_a|e\rangle_b+\sqrt{\epsilon}|e\rangle_a|\downarrow\rangle_b+\epsilon|e\rangle_a|e\rangle_b$. For successful atom–atom entanglement, a single photon must be detected from one of the two atoms, where the detector is only sensitive to the $|e\rangle\rightarrow|\uparrow\rangle$ decay channel. If the atomic excitation is sufficiently small such that the probability of both atoms emitting a photon is negligible, $\epsilon^2\ll 2\epsilon$, then by the projection postulate, after detection of the single photon, the atoms are in the en-

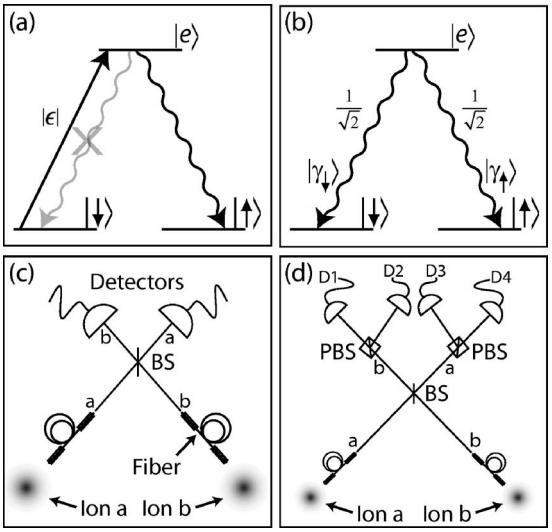

Fig. 2. Entanglement schemes for two remotely located atomic qubits. (a) In the single-photon protocol by Cabrillo *et al.* (Ref. 55), each atom is weakly excited with a probability ϵ from the ground state $|\downarrow\rangle$ to the excited state $|e\rangle$. The photon detectors are only sensitive to the $|e\rangle$ to $|\uparrow\rangle$ decay, and a detection of a single photon projects the atoms into the entangled state $(|\downarrow\rangle_a|\uparrow\rangle_b + e^{i\phi}|\uparrow\rangle_a|\downarrow\rangle_b)/\sqrt{2}$. (b) In the two-photon protocol, each atom is prepared in the excited state with two decay channels giving rise to two distinguishable photonic qubit states. (c) Detection setup suitable for either entanglement protocol. With the protocol by Cabrillo *et al.*, only one of the two detectors detects a photon; whereas the two-photon protocol requires coincident detection on each detector projecting the atoms into the entangled Bell state $|\Psi^-\rangle_{\text{atom}} = (|\uparrow\rangle_a|\downarrow\rangle_b - |\downarrow\rangle_a|\uparrow\rangle_b)/\sqrt{2}$. (d) Alternative setup when using polarization qubits in the two-photon protocol. Coincident detection between D1 and D3 or D2 and D4 projects the atoms into the state $|\Psi^-\rangle_{\text{atom}}$, whereas coincident detection between D1 and D2 or D3 and D4 results in $|\Psi^+\rangle_{\text{atom}} = (|\uparrow\rangle_a|\downarrow\rangle_b + |\downarrow\rangle_a|\uparrow\rangle_b)/\sqrt{2}$.

tangled state $(|\downarrow\rangle_a|\uparrow\rangle_b + e^{i\phi}|\uparrow\rangle_a|\downarrow\rangle_b)/\sqrt{2}$ where the phase $\phi = k\Delta x$ comes from the optical path length difference between each atom and the detector.

One limitation to the entanglement fidelity achievable with this protocol is the probability of multiple photon emissions. By choosing $\epsilon \ll 1$, this probability is lowered but at the expense of lowering the entanglement success probability. This protocol also requires that the atoms must be well localized such that the path length the photon travels to the detector is known much better than the wavelength of the emitted photon.[58,59] Otherwise, the phase in the final entangled state will be unknown and will ruin entanglement. Similarly, if an atom experiences a recoil upon emission, the evidence of which atom emitted the photon will again ruin the entanglement fidelity. These last two restrictions, however, may be overcome if the atoms are localized to well within the Lamb–Dicke limit.

A more robust two-photon protocol for remote-atom entanglement, not requiring localization within the Lamb–Dicke limit and insensitive to the photonic phase, was proposed independently by Duan and Kimble[56] and Simon and Irvine.[57] The atomic energy levels for this approach are the same as the previous protocol, but the excited state is prepared with arbitrarily high probability and requires the coincident detection of two photons, one from each atom [Fig. 2(b)]. The excited state has two decay channels with distinguishable photonic qubit modes—either polarization or frequency modes. After simultaneous excitations, the atoms each emit a single photon and are in the state:

$$\begin{aligned}&\tfrac{1}{2}(|\downarrow\rangle_a|\gamma_\downarrow\rangle_a + |\uparrow\rangle_a|\gamma_\uparrow\rangle_a) \otimes (|\downarrow\rangle_b|\gamma_\downarrow\rangle_b + |\uparrow\rangle_b|\gamma_\uparrow\rangle_b)\\ &\quad = \tfrac{1}{2}(|\Psi^+\rangle_{\text{atom}}|\Psi^+\rangle_{\text{photon}} + |\Psi^-\rangle_{\text{atom}}|\Psi^-\rangle_{\text{photon}}\\ &\qquad + |\Phi^+\rangle_{\text{atom}}|\Phi^+\rangle_{\text{photon}} + |\Phi^-\rangle_{\text{atom}}|\Phi^-\rangle_{\text{photon}}),\end{aligned} \tag{2}$$

where $|\gamma_\downarrow\rangle$ and $|\gamma_\uparrow\rangle$ represent the photonic qubit, and $|\Psi^\pm\rangle_{\text{atom}} = (|\uparrow\rangle_a|\downarrow\rangle_b \pm |\downarrow\rangle_a|\uparrow\rangle_b)/\sqrt{2}$, and $|\Phi^\pm\rangle_{\text{atom}} = (|\uparrow\rangle_a|\uparrow\rangle_b \pm |\downarrow\rangle_a|\downarrow\rangle_b)/\sqrt{2}$ are the maximally entangled Bell states for the atoms (with similar definitions for the photons). If the two photon modes are matched on a 50/50 BS, then they will exit on different ports only if they are in the antisymmetric state $|\Psi^-\rangle_{\text{photon}} = (|\gamma_\uparrow\rangle_a|\gamma_\downarrow\rangle_b - |\gamma_\downarrow\rangle_a|\gamma_\uparrow\rangle_b)/\sqrt{2}$ respecting the symmetry of the overall photonic wave function.[60] Therefore, coincident photon detection in the two output ports of this BS projects the atoms into $|\Psi^-\rangle_{\text{atom}}$ [Fig. 2(c)]. Additionally, with a polarizing BS placed in either output port, it is possible to detect the (polarization qubit) photons in the state $|\Psi^+\rangle_{\text{photon}}$ thus projecting the atoms into the state $|\Psi^+\rangle_{\text{atom}}$ [Fig. 2(d)]. For the other two photonic Bell states $|\Phi^\pm\rangle_{\text{photon}}$, both photons always go to one detector and thus cannot herald a unique entangled state of the atoms.[57]

For high fidelity atom–atom entanglement, it is important to emit only a single photon from each atom. With atom–photon entanglement, good entanglement fidelities can still be obtained using weak cw excitations, where the probability of spontaneously emitting two photons is $p_{2e} = p_e^2/2$. Hence, when detecting a single photon, the probability of a second emitted photon, potentially affecting the fidelity of the entanglement, is only $p_e/2$. However, in the two photon atom–atom entanglement protocol, the probability of two photons being detected from one atom is of the same order as detecting two photons from different atoms (discussed in more detail in the next section). Emitting only a single photon requires the excitation pulse duration to be much shorter than the excited state lifetime and allows for $p_{2e} \to 0$. In addition to eliminating multiple excitations, a fast excitation pulse can also allow for near-unit-excitation probability ($p_e \sim 1$), which can lead to a significant increase in entanglement success probability.

With the right parameters, one could allow for quantum gates between the atoms using this protocol.[30] For this, the choice of pulse length (bandwidth) must allow for unique simultaneous excitation of all hyperfine states.[30] Therefore, the pulsed laser bandwidth needs to be larger than the largest hyperfine splitting but smaller than the fine structure splitting to eliminate coupling to the different excited state levels (Fig. 3).

Since the probability of detecting a single emitted photon is typically low, the requirement to detect two such photons can make this protocol significantly slower than the single-photon protocol. However, with the possibility to considerably increase the effective photon collection

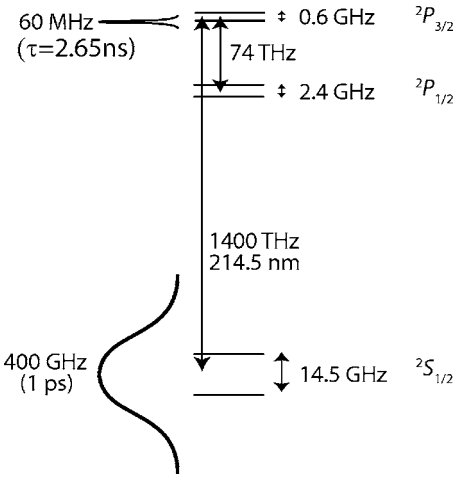

Fig. 3. Energy levels (not to scale) and laser bandwidth requirements for the generation of a high efficiency single-photon source (atomic values shown are for $^{111}Cd^+$). For simultaneous excitation of all hyperfine states, the bandwidth of the laser pulse must be much larger than the largest hyperfine splitting but smaller than the fine structure splitting to eliminate coupling to the different excited state levels. To eliminate multiple scatters, the pulse duration must be much smaller than the excited state lifetime (have a bandwidth much larger than the linewidth of the excited state).

solid angle via an optical cavity, the latter approach can be comparable in success probability (or even greater if the atoms are excited with unit probability) due to the intrinsic limitation of $p_e \ll 1$ in the single-photon protocol.

4. COUPLING PHOTON MODES WITH A BEAM SPLITTER

The central component of the photonic coupling used to entangle atomic qubits is the interference of photons on a BS. This involves single photons entering the two input ports of the BS as shown in Fig. 4. If the spatial and temporal modes of the two photons coincide on the BS, there are two indistinguishable ways for the photons to emerge in separate output ports: both photons are transmitted through the BS, and both photons are reflected from the BS [Figs. 4(d) and 4(e)]. It is the destructive interference of these two amplitudes[60] that can project the atoms into an entangled state.

We consider the general interference of two photonic modes on a BS, which can be conveniently described by effective angular momentum rotation operators.[61] As shown in Fig. 4(a), spatial modes a and b are depicted by the two straight paths through the BS, and the BS transfers photons between these two modes. Given n and m photons in respective modes a and b before the BS, the action of the BS is identical to rotations within an effective $J=N/2$ angular momentum system where $N=n+m$. Formally, the two-mode input state $|n\rangle_a|m\rangle_b$ evolves to

$$|n\rangle_a|m\rangle_b \rightarrow e^{-i\chi\hat{J}_y}|n\rangle_a|m\rangle_b, \tag{3}$$

where the rotation angle χ is π times the reflectivity R of the lossless BS, and $\hat{J}_y=-i(\hat{a}^\dagger\hat{b}-\hat{a}\hat{b}^\dagger)/2$.[61] The photon annihilation and creation operators, $\hat{a}$ and $\hat{a}^\dagger$ for modes a and $\hat{b}$ and $\hat{b}^\dagger$ for mode b, follow the usual bosonic commutation relations $[\hat{a},\hat{a}^\dagger]=[\hat{b},\hat{b}^\dagger]=1$.

We write down the evolution of two-mode photonic states for up to $N=2$ total photons using angular momentum rotation matrices.[62] Obviously, the trivial case of $N=0$ photons does not evolve. For a total of $N=1$ photon in the two input modes, we find that the equivalent spin-1/2 system evolves as

$$\begin{pmatrix} |0\rangle_a|1\rangle_b \\ |1\rangle_a|0\rangle_b \end{pmatrix} \rightarrow \begin{bmatrix} \cos\frac{\chi}{2} & \sin\frac{\chi}{2} \\ -\sin\frac{\chi}{2} & \cos\frac{\chi}{2} \end{bmatrix} \begin{pmatrix} |0\rangle_a|1\rangle_b \\ |1\rangle_a|0\rangle_b \end{pmatrix}. \tag{4}$$

For $N=2$ photon input states, we similarly find

$$\begin{pmatrix} |0\rangle_a|2\rangle_b \\ |1\rangle_a|1\rangle_b \\ |2\rangle_a|0\rangle_b \end{pmatrix} \rightarrow \begin{bmatrix} \frac{1}{2}(1+\cos\chi) & \frac{1}{\sqrt{2}}\sin\chi & \frac{1}{2}(1-\cos\chi) \\ \frac{-1}{\sqrt{2}}\sin\chi & \cos\chi & \frac{1}{\sqrt{2}}\sin\chi \\ \frac{1}{2}(1-\cos\chi) & \frac{-1}{\sqrt{2}}\sin\chi & \frac{1}{2}(1+\cos\chi) \end{bmatrix} \times \begin{pmatrix} |0\rangle_a|2\rangle_b \\ |1\rangle_a|1\rangle_b \\ |2\rangle_a|0\rangle_b \end{pmatrix}. \tag{5}$$

As discussed previously, when an atom emits a photon, attributes of the photon (e.g., polarization or frequency) can become entangled with the atomic qubit, spanned by

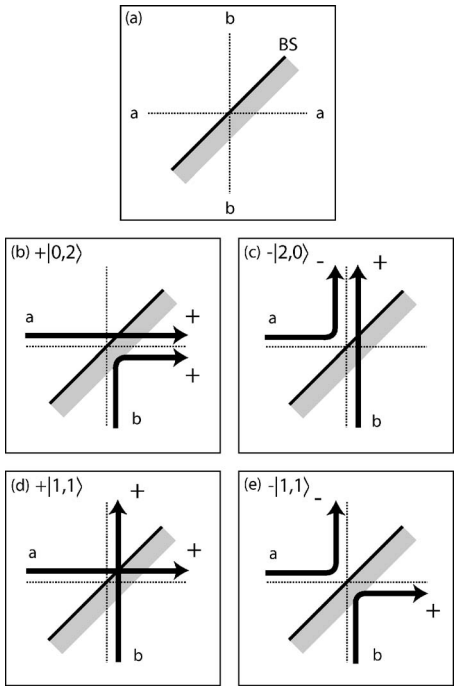

Fig. 4. (a) Spatial modes a and b are straight paths through the BS, and the BS interferes with these two modes. (b)–(e) Four possible output modes of two photons entering a BS from different ports. A negative phase is acquired only upon reflection from low to high index of refraction—mode a in (c) and (e).

the atomic qubit states $|\downarrow\rangle$ and $|\uparrow\rangle$. This internal degree of freedom of the photon (photonic qubit) is represented by the two states $q=\alpha,\beta$ in a given spatial mode $s=a,b$. We begin with a description of the quantum state of a single atomic qubit and the photonic mode into which the atom emits, including various imperfections such as background light and multiple atomic excitations. We then extend this situation to the case of two atoms whose emitted photons interact on a BS following the above transformations.

A single atom is prepared in its excited state with excitation probability p_e, given one of the atomic level schemes in Fig. 1, with a probability of double sequential excitation $p_{2e} \ll p_e$. For a weak excitation pulse of duration $t_e > \tau$, $p_e \ll 1$, and $p_{2e}=p_e^2/2$, while for an ultrafast excitation where $t_e \ll \tau$, we expect $p_{2e} \sim t_e/\tau \ll p_e^2/2$. Given that the atom is excited, the probability p that a single photon is detected in mode s is determined by the overlap between the atomic emission mode and spatial mode s in addition to transmission losses and the detection efficiency as discussed previously. (We assume that $p \ll 1$, but this analysis applies equally well to cases where $p \approx 1$, appropriate for cavity-QED setups, where the atom preferentially emits into mode s.) The desired (postselected) atom–photon entangled state is of the form

$$|\Psi^{\mathrm{ent}}\rangle = \cos\theta_s|\downarrow\rangle_s|0\rangle_s^{\alpha}|1\rangle_s^{\beta} + \sin\theta_s|\uparrow\rangle_s|1\rangle_s^{\alpha}|0\rangle_s^{\beta}, \qquad (6)$$

where $|n\rangle_s^q$ is a state of n photons in spatial mode s and internal photonic qubit state q. The parameter θ_s depends on the particular excitation scheme (Fig. 1) and is usually near $\pi/4$. For ultrafast excitation schemes, θ_s may describe the initial atomic qubit state that is mapped onto the atom–photon entangled state.[30,49] After a repetition time T_{rep} long enough for the spontaneous emission of a photon, the complete quantum state of the atom–photon system is a mixed state of several alternatives with respective probabilities given in Table 1.

The first term in Table 1 corresponds to the typical case of zero photons in either qubit state α or qubit state β resulting in a random atomic qubit state $|M\rangle_s=|\downarrow\rangle_s$ or $|\uparrow\rangle_s$, while the second term corresponds to the desired creation of entanglement between the atomic qubit and a single photonic qubit. The remaining terms are errors occurring from background events (background light entering the photonic mode) with probability pp_{bg} and multiple excitation events with probability pp_{2e} and p^2p_{2e} corresponding to the detection of one or both emitted photons, respectively. Here, $p_{bg} \ll 1$ is the ratio of background photons to atomic fluorescence photons detected in time T_{rep}. These error events are assumed to have an effective 50% chance of populating either photonic qubit state α or photonic qubit state β of spatial mode s, and multiple excitations are assumed to result in a random mixed state $|M\rangle_s=|\downarrow\rangle_s$ or $|\uparrow\rangle_s$. The error states listed are the lowest-order possibilities in their respective probabilities ($p, p_{bg}, p_{2e} \ll 1$).

When each of two atom–photon systems is independently and simultaneously prepared in the above form, the photonic part of these states can be interfered on a BS, and subsequent detection of the photons after the BS can project entanglement between the atoms. We now describe the quantum state of the atoms and photons after the BS under the assumption that only photons with identical internal modes α or β (e.g., the two states of polarization or frequency) interfere on the BS according to the transformations in Eqs. (4) and (5). In general, we assume that the two atoms are prepared in unique entangled superpositions with their photons represented by the two angles θ_a and θ_b. Anticipating the postselection of states that result in two photons leaving the BS in distinct modes (either in separate spatial modes or in the same spatial mode but with distinct internal modes), we write down only those states and their associated probabilities after time T_{rep} in Table 2.

In Table 2, the desired atom–atom entangled states are

$$|\Psi^{\beta\alpha}\rangle_{ab} = \mathcal{N}_1\left(\cos\theta_a \sin\theta_b \cos^2\frac{\chi}{2}|\downarrow\rangle_a|\uparrow\rangle_b - \sin\theta_a \cos\theta_b \sin^2\frac{\chi}{2}|\uparrow\rangle_a|\downarrow\rangle_b\right), \qquad (7)$$

Table 1. Mixed Quantum State of a Single Atom and a Single Photon of Spatial Mode s after Time T_{rep} Longer than the Spontaneous Emission Lifetime of the Atom[a]

Quantum State	Probability	Description
$\|M\rangle_s\|0\rangle_s^{\alpha}\|0\rangle_s^{\beta}$	$1-pp_e-pp_{bg}$	No photons
$\cos\theta_s\|\downarrow\rangle_s\|0\rangle_s^{\alpha}\|1\rangle_s^{\beta}+\sin\theta_s\|\downarrow\rangle_s\|1\rangle_s^{\alpha}\|0\rangle_s^{\beta}$	pp_e	Good photon
$\|M\rangle_s\|0\rangle_s^{\alpha}\|1\rangle_s^{\beta}$	$\frac{1}{2}pp_{bg}$	Background photon
$\|M\rangle_s\|1\rangle_s^{\alpha}\|0\rangle_s^{\beta}$	$\frac{1}{2}pp_{bg}$	Background photon
$\|M\rangle_s\|0\rangle_s^{\alpha}\|2\rangle_s^{\beta}$	$\frac{1}{4}p^2p_{bg}^2$	Background photons
$\|M\rangle_s\|2\rangle_s^{\alpha}\|0\rangle_s^{\beta}$	$\frac{1}{4}p^2p_{bg}^2$	Background photons
$\|M\rangle_s\|1\rangle_s^{\alpha}\|1\rangle_s^{\beta}$	$\frac{1}{2}p^2p_{bg}^2$	Background photons
$\cos\theta_s\|\downarrow\rangle_s\|1\rangle_s^{\alpha}\|1\rangle_s^{\beta}+\sin\theta_s\|\downarrow\rangle_s\|2\rangle_s^{\alpha}\|0\rangle_s^{\beta}$	$\frac{1}{2}p^2p_ep_{bg}$	Background+good photons
$\cos\theta_s\|\downarrow\rangle_s\|0\rangle_s^{\alpha}\|2\rangle_s^{\beta}+\sin\theta_s\|\downarrow\rangle_s\|1\rangle_s^{\alpha}\|1\rangle_s^{\beta}$	$\frac{1}{2}p^2p_ep_{bg}$	Background+good photons
$\|M\rangle_s\|0\rangle_s^{\alpha}\|1\rangle_s^{\beta}$	pp_{2e}	Double-excitation photon
$\|M\rangle_s\|1\rangle_s^{\alpha}\|0\rangle_s^{\beta}$	pp_{2e}	Double-excitation photon
$\|M\rangle_s\|0\rangle_s^{\alpha}\|2\rangle_s^{\beta}$	$\frac{1}{4}p^2p_{2e}$	Double-excitation photons
$\|M\rangle_s\|2\rangle_s^{\alpha}\|0\rangle_s^{\beta}$	$\frac{1}{4}p^2p_{2e}$	Double-excitation photons
$\|M\rangle_s\|1\rangle_s^{\alpha}\|1\rangle_s^{\beta}$	$\frac{1}{2}p^2p_{2e}$	Double-excitation photons

[a]The atomic qubit is represented by states $|\uparrow\rangle_s$ and $|\downarrow\rangle_s$ ($|M\rangle_s$ is an equal mixture of the two atomic qubit states), and the photon mode can support photons of internal qubit states α and β. The lowest-order possibilities are listed with their associated probabilities.

Table 2. Mixed Quantum State of Two Photon Modes and Two Atomic Qubits Given that Two Atom–Photon Systems are Prepared According to Table 1 and the Photon Modes are Coupled on a BS[a]

Photonic State	Atomic State	Probability
$(\|0\rangle_a^\alpha\|1\rangle_a^\beta)$ $(\|1\rangle_b^\alpha\|0\rangle_b^\beta)$	$\|\Psi^{\beta\alpha}\rangle_{ab}$	$p^2p_e^2\left(\cos^2\theta_a\sin^2\theta_b\cos^4\frac{\chi}{2}+\sin^2\theta_a\cos^2\theta_b\sin^4\frac{\chi}{2}\right)$
	$\|M\rangle_a\|M\rangle_b$	$p^2\left\{\frac{1}{4}p_{bg}^2\left(1+\frac{\sin^2\chi}{2}\right)+\frac{1}{2}p_{bg}p_e\left[1+(\cos 2\theta_a-\cos 2\theta_b)\frac{\cos\chi}{2}\right]\right.$ $+p_{2e}p_{bg}\left(1-\frac{\sin^2\chi}{2}\right)+p_{2e}p_e\left[1-\frac{\sin^2\chi}{2}+(\cos 2\theta_a-\cos 2\theta_b)\frac{\cos\chi}{2}\right]$ $\left.+\frac{1}{4}p_{2e}\sin^2\chi\right\}$
$(\|1\rangle_a^\alpha\|0\rangle_a^\beta)$ $(\|0\rangle_b^\alpha\|1\rangle_b^\beta)$	$\|\Psi^{\alpha\beta}\rangle_{ab}$	$p^2p_e^2\left(\cos^2\theta_a\sin^2\theta_b\sin^4\frac{\chi}{2}+\sin^2\theta_a\cos^2\theta_b\cos^4\frac{\chi}{2}\right)$
	$\|M\rangle_a\|M\rangle_b$	$p^2\left\{\frac{1}{4}p_{bg}^2\left(1+\frac{\sin^2\chi}{2}\right)+\frac{1}{2}p_{bg}p_e\left[1-(\cos 2\theta_a-\cos 2\theta_b)\frac{\cos\chi}{2}\right]\right.$ $+p_{2e}p_{bg}\left(1-\frac{\sin^2\chi}{2}\right)+p_{2e}p_e\left[1-\frac{\sin^2\chi}{2}-(\cos 2\theta_a-\cos 2\theta_b)\frac{\cos\chi}{2}\right]$ $\left.+\frac{1}{4}p_{2e}\sin^2\chi\right\}$
$(\|1\rangle_a^\alpha\|1\rangle_a^\beta)$ $(\|0\rangle_b^\alpha\|0\rangle_b^\beta)$	$\|\Psi^{\alpha\beta}\rangle_{aa}$	$\frac{1}{4}p^2p_e^2(\cos^2\theta_a\sin^2\theta_b+\sin^2\theta_a\cos^2\theta_b)\sin^2\chi$
	$\|M\rangle_a\|M\rangle_b$	$\frac{1}{2}p^2\left[\frac{1}{2}p_{bg}^2\left(2-\frac{\sin^2\chi}{2}\right)+p_{bg}p_e+p_{2e}(p_{bg}+p_e)\sin^2\chi+p_{2e}\left(1-\frac{\sin^2\chi}{2}\right)\right]$
$(\|0\rangle_a^\alpha\|0\rangle_a^\beta)$ $(\|1\rangle_b^\alpha\|1\rangle_b^\beta)$	$\|\Psi^{\alpha\beta}\rangle_{bb}$	$\frac{1}{4}p^2p_e^2(\cos^2\theta_a\sin^2\theta_b+\sin^2\theta_a\cos^2\theta_b)\sin^2\chi$
	$\|M\rangle_a\|M\rangle_b$	$\frac{1}{2}p^2\left[\frac{1}{2}p_{bg}^2\left(2-\frac{\sin^2\chi}{2}\right)+p_{bg}p_e+p_{2e}(p_{bg}+p_e)\sin^2\chi+p_{2e}\left(1-\frac{\sin^2\chi}{2}\right)\right]$
$(\|0\rangle_a^\alpha\|1\rangle_a^\beta)$ $(\|0\rangle_b^\alpha\|1\rangle_b^\beta)$	$\|\downarrow\rangle_a\|\downarrow\rangle_b$	$p^2p_e^2\cos^2\theta_a\cos^2\theta_b\cos^2\chi$
	$\|M\rangle_a\|M\rangle_b$	$p^2\left\{\frac{1}{4}p_{bg}^2+\frac{1}{4}p_{bg}p_e(\cos^2\theta_a+\cos^2\theta_b)(1+\cos^2\chi)\right.$ $\left.+p_{2e}[p_{bg}+p_e(\cos^2\theta_a+\cos^2\theta_b)]\cos^2\chi+\frac{1}{4}p_{2e}\sin^2\chi\right\}$
$(\|1\rangle_a^\alpha\|0\rangle_a^\beta)$ $(\|1\rangle_b^\alpha\|0\rangle_b^\beta)$	$\|\uparrow\rangle_a\|\uparrow\rangle_b$	$p^2p_e^2\sin^2\theta_a\sin^2\theta_b\cos^2\chi$
	$\|M\rangle_a\|M\rangle_b$	$p^2\left\{\frac{1}{4}p_{bg}^2+\frac{1}{4}p_{bg}p_e(\sin^2\theta_a+\sin^2\theta_b)(1+\cos^2\chi)\right.$ $\left.+p_{2e}[p_{bg}+p_e(\sin^2\theta_a+\sin^2\theta_b)]\cos^2\chi+\frac{1}{4}p_{2e}\sin^2\chi\right\}$

[a]The BS has reflectivity $R=\chi/\pi$, and only those states with two single photons emerging in distinct modes are written with their associated probabilities. Higher-order processes in the probabilities p, p_{bg}, and p_{2e} are not listed.

$$|\Psi^{\alpha\beta}\rangle_{ab}=\mathcal{N}_2\left(\cos\theta_a\sin\theta_b\sin^2\frac{\chi}{2}|\downarrow\rangle_a|\uparrow\rangle_b-\sin\theta_a\cos\theta_b\cos^2\frac{\chi}{2}|\uparrow\rangle_a|\downarrow\rangle_b\right), \tag{8}$$

$$|\Psi^{\alpha\beta}\rangle_{aa}=\mathcal{N}_3[(\cos\theta_a\sin\theta_b|\downarrow\rangle_a|\uparrow\rangle_b+\sin\theta_a\cos\theta_b|\uparrow\rangle_a|\downarrow\rangle_b)\sin\chi], \tag{9}$$

$$|\Psi^{\alpha\beta}\rangle_{bb}=|\Psi^{\alpha\beta}\rangle_{aa}, \tag{10}$$

where $\mathcal{N}_i$ are normalization constants. The first two states are correlated with single photons emerging in the two different BS spatial modes a and b having opposite photonic qubit states, and the last two states are correlated with single photons emerging in the same output port of the BS again with opposite photonic qubit states. As shown in Fig. 2(d) for the case of polarization photonic qubit states, these four outcomes can be uniquely deter-

mined by separating the photonic qubit states at the output of each BS output port and triggering on the relevant two-photon coincidence event.

For a 50/50 BS ($\chi=\pi/2$), the above states simplify to one of the following entangled states:

$$|\Psi^{\mathrm{ent}}\rangle_{\mathrm{diff}}=\mathcal{N}(\cos\theta_a\sin\theta_b|\downarrow\rangle_a|\uparrow\rangle_b-\sin\theta_a\cos\theta_b|\uparrow\rangle_a|\downarrow\rangle_b), \tag{11}$$

$$|\Psi^{\mathrm{ent}}\rangle_{\mathrm{same}}=\mathcal{N}(\cos\theta_a\sin\theta_b|\downarrow\rangle_a|\uparrow\rangle_b+\sin\theta_a\cos\theta_b|\uparrow\rangle_a|\downarrow\rangle_b), \tag{12}$$

where $\mathcal{N}$ is a normalization constant, and the subscripts "diff" and "same" refer to cases where the two photons emerged in different spatial modes or the same spatial mode but separate photonic qubit states. This postselection process can amount to a measurement gate between the two atoms originally prepared in arbitrary states given by θ_a and θ_b.[30] For $\theta_a=\theta_b$ (identically prepared atoms), the above states simplify to the odd-parity Bell states $|\Psi^-\rangle_{\mathrm{atom}}=(|\downarrow\rangle_a|\uparrow\rangle_b-|\uparrow\rangle_a|\downarrow\rangle_b)/\sqrt{2}$ and $|\Psi^+\rangle_{\mathrm{atom}}=(|\downarrow\rangle_a|\uparrow\rangle_b+|\uparrow\rangle_a|\downarrow\rangle_b)/\sqrt{2}$, respectively.

When the BS is not exactly 50/50 ($\chi\neq\pi/2$), the resulting errors can limit the fidelity of the gate or the entangled state. By detecting all possibilities of photonic output states, a biased BS can be diagnosed by the appearance of events with identical photonic qubit states emerging in distinct BS output ports (last two rows of Table 2) assuming that errors from background counts or double-excitation events are rare. In the following, we therefore assume that the BS is unbiased ($\chi=\pi/2$).

Including noise from background counts and double excitations, we find that when two photons are detected in coincidence in the desired output ports of the BS (for either the $|\Psi^{\mathrm{ent}}\rangle_{\mathrm{diff}}$ or the $|\Psi^{\mathrm{ent}}\rangle_{\mathrm{same}}$ state), the postselected mixed state of the two atoms alone becomes

$$\rho_{\mathrm{post}}=P_{\mathrm{good}}|\Psi^{\mathrm{ent}}\rangle\langle\Psi^{\mathrm{ent}}|+P_{\mathrm{bad}}|M_aM_b\rangle\langle M_aM_b|, \tag{13}$$

where the probabilities of a desired entangled state P_{good} and the noisy mixed state P_{bad} are given by

$$P_{\mathrm{good}}=\frac{1}{4}p^2p_e^2(\cos^2\theta_a\sin^2\theta_b+\sin^2\theta_a\cos^2\theta_b), \tag{14}$$

$$P_{\mathrm{bad}}=\frac{p^2}{2}\left[p_{bg}\left(\frac{3}{4}p_{bg}+p_e\right)+p_{2e}\left(p_{bg}+p_e+\frac{1}{2}\right)\right]. \tag{15}$$

The above probabilities do not add to one because they are relative to the (most probable) null case of not detecting photons in each of the output modes of the BS. Nevertheless, we can calculate a lower limit on the fidelity of the heralded entangled atomic qubit state most importantly for the maximally entangled Bell states $|\Psi^-\rangle_{\mathrm{atom}}$ and $|\Psi^+\rangle_{\mathrm{atom}}$ ($\theta_a=\theta_b=\pi/4$). Noting that the fidelity of the random mixed state $|M_aM_b\rangle$ is 1/4, we find that the fidelity of the postselected state is

$$\mathcal{F}=\frac{P_{\mathrm{good}}+\frac{1}{4}P_{\mathrm{bad}}}{P_{\mathrm{good}}+P_{\mathrm{bad}}}=\frac{p_e^2+\left[p_{bg}\left(\frac{3}{4}p_{bg}+p_e\right)+p_{2e}\left(p_{bg}+p_e+\frac{1}{2}\right)\right]}{p_e^2+4\left[p_{bg}\left(\frac{3}{4}p_{bg}+p_e\right)+p_{2e}\left(p_{bg}+p_e+\frac{1}{2}\right)\right]}. \tag{16}$$

One criterion for the generation of entanglement is that the fidelity be greater than 1/2, which leads to the condition that $P_{\mathrm{good}}>P_{\mathrm{bad}}/2$, or $p_e^2>2p_{bg}(\frac{3}{4}p_{bg}+p_e)+2p_{2e}(p_{bg}+p_e+\frac{1}{2})$. It is clear that when using a weak excitation pulse of duration $t_e>\tau$, the entanglement fidelity is severely limited ($P_{\mathrm{bad}}\approx P_{\mathrm{good}}$), since $p_{2e}=p_e^2/2$. However, when using ultrafast excitation pulses such that $p_e\to 1$ and $p_{2e}\to 0$, only the background photons can affect the resulting fidelity: $\mathcal{F}\sim 1-3p_{bg}$.

5. EXPERIMENTS WITH PHOTON POLARIZATION QUBITS

While matter–light entanglement has been implicit in many experimental systems over the past few decades,[58,63–77] the first system with sufficient control for direct measurement of entanglement between matter and light was the trapped ion system.[73,74] In this system, a photon is spontaneously emitted from a single trapped atomic ion, which is initially excited to a state with two decay channels, resulting in photons of different polarizations [Fig. 1(b)].

A diagram of the relevant energy levels and a description of the experiment with a single $^{111}Cd^+$ ion is shown in Fig. 5. First, the ion is optically pumped to the $^2S_{1/2}$ $|0,0\rangle$ state followed by a microwave pulse that drives the population to $|1,0\rangle$. From here, an approximately 50 ns pulse of σ^+-polarized laser light resonant with the $^2S_{1/2}$ $F=1\leftrightarrow{}^2P_{3/2}$ $F=2$ transition weakly excites the ion to the $^2P_{3/2}$ $|2,1\rangle$ state, which has a radiative lifetime of 2.65 ns.[78] As described earlier, the ion decays via two channels to the ground state and if viewed perpendicularly to the quantization axis creates the entangled state $\sqrt{1/3}|H\rangle|\downarrow\rangle+\sqrt{2/3}|V\rangle|\uparrow\rangle$.

The collected light passes through a $\lambda/2$ wave plate for polarization rotation, and the resulting polarization state is measured by a polarizing BS and two photomultiplier tubes (PMTs). Upon the detection of a photon on either PMT, manipulation of the ion is performed. First, the qubit is transferred to the clock states via a microwave pulse driving the $|1,1\rangle$ population to the $|0,0\rangle\equiv|\tilde{\uparrow}\rangle$ state. A second microwave pulse resonant with the $|\downarrow\rangle\leftrightarrow|\tilde{\uparrow}\rangle$ transition with adjustable phase and pulse length subsequently rotates the atomic qubit to any desired measurement basis, and the resulting state is measured with a σ^+-polarized laser pulse via standard trapped ion resonance fluorescence techniques.[79,80] The resulting fidelity is measured to be $\geqslant 87\%$. Factors contributing to the resulting fidelity compared to the possible 97% include: multiple excitations of the ion during the cw pump pulse (2.5%), mixing of photon polarizations due to the nonzero solid angle (0.5%), imperfect atomic and photonic qubit rotations (1.5%), background PMT counts leading to false positives (5%–10%), and imperfections in the polarization

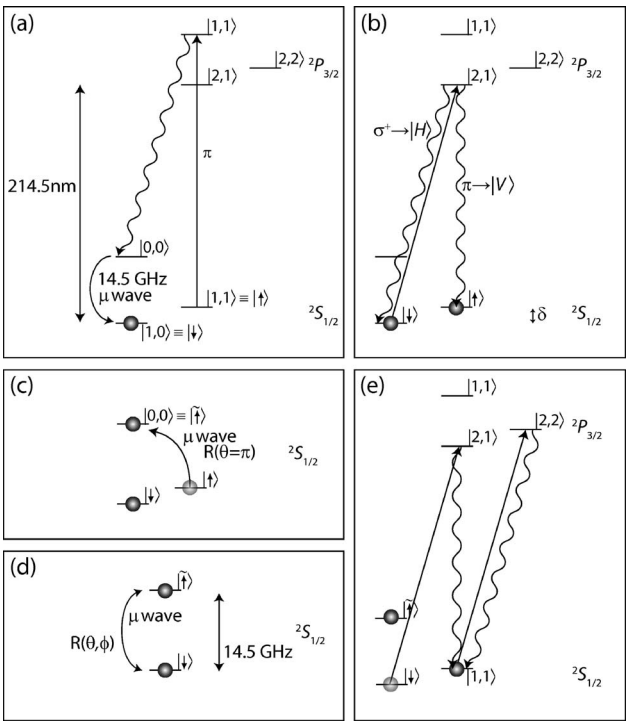

Fig. 5. Experimental procedure for atom–photon entanglement with photon polarization qubits (Refs. 73 and 74). (a) The atom is initialized to the $|1,0\rangle$ state via optical pumping to the $|0,0\rangle$ state and a microwave transfer pulse. (b) The atom is driven to the $^2P_{3/2}$ $|2,1\rangle$ excited state resulting in spontaneous emission via two photon decay channels of orthogonal polarizations when viewed perpendicularly to the quantization axis. The resulting entangled state is $\sqrt{1/3}|H\rangle|\downarrow\rangle+\sqrt{2/3}|V\rangle|\uparrow\rangle$. (c) Microwave ($\mu$wave) pulse resonant with the $|1,1\rangle \leftrightarrow |0,0\rangle$ transition coherently transfers the population to the clock qubit states. (d) Second microwave pulse prepares the atomic qubit for measurement in any basis. (e) σ^+-polarized laser pulse performs the state detection of the atomic qubit using resonance fluorescence techniques.

optics (3%). Since the qubit is transferred to the clock qubit states right after photon emission, we estimate that magnetic field fluctuations affect the atomic qubit fidelity by $\ll 1\%$. When combined, these sources of error are consistent with the observed fidelity.

As mentioned above, this entanglement generation is a probabilistic process. With the cw excitation scheme, the probability of emitting a single photon in each trial is restricted to $p_e \approx 0.1$ to suppress multiple excitations. The resulting success probability is $P_{\mathrm{a-p}}=p_e \eta T(\Delta\Omega/4\pi)=(0.1)\times(0.2)(0.4)(0.02)\approx 1.6\times 10^{-4}$. The experiment repetition rate is $R=1/T_{\mathrm{rep}}=10^4\ \mathrm{s}^{-1}$ resulting in an entanglement generation rate $R_{\mathrm{a-p}}=P_{\mathrm{a-p}}R\approx 1.6\ \mathrm{s}^{-1}$, but improvements such as higher excitation probability using an ultrafast laser pulse and an increased repetition rate significantly increase this yield.

6. EXPERIMENTS WITH PHOTON FREQUENCY QUBITS

In a recent experiment, indirect evidence of the entanglement between an atomic qubit and a photon frequency qubit was demonstrated in the cadmium ion system.[49] A diagram of the relevant energy levels and a description of the experiment are given in Fig. 6. First, the ion is optically pumped to $|0,0\rangle \equiv |\uparrow\rangle$, and a microwave pulse prepares the ion in the state $(|\downarrow\rangle+|\uparrow\rangle)/\sqrt{2}$ [Fig. 6(a)].

Next, a single π-polarized ultrafast laser pulse coherently drives the superposition to the clock states in the $^2P_{3/2}$ manifold with near-unit probability—similar to the scheme described in Section 2 [Fig. 1(f)]. The coherence

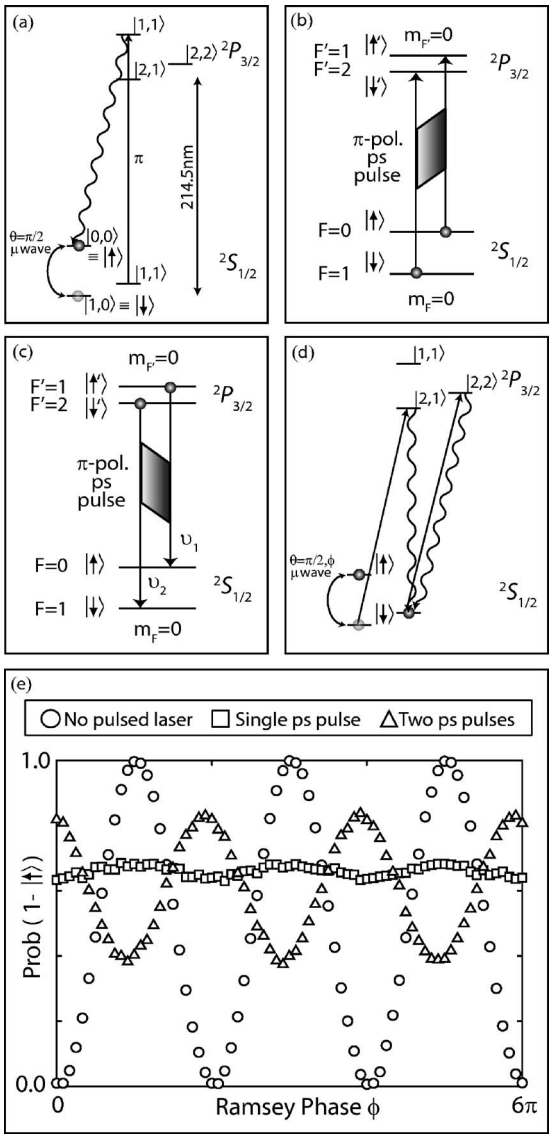

Fig. 6. Experimental procedure for atom–photon entanglement with photon frequency qubits (Ref. 49). (a) The ion is initialized in the state $(|\downarrow\rangle+|\uparrow\rangle)/\sqrt{2}$ via optical pumping to the $|0,0\rangle$ state and a microwave $\pi/2$ pulse. (b) Superposition of atomic qubit states is coherently driven to the $^2P_{3/2}$ excited state via a resonantly tuned π-polarized ultrafast laser pulse. (c) Second pulse drives the qubit back to the ground state a short time later. (d) Second $\pi/2$ microwave pulse with variable phase completes the Ramsey experiment, and the atomic state is measured using a resonance fluorescence technique. (e) Results from the microwave Ramsey experiment. Circles show the near perfect Ramsey fringes for the case with no ultrafast laser pulse. With a single ultrafast laser pulse, the coherence is lost due to the spontaneous emission of a photon that is not measured in a controlled, precisely timed fashion (squares). The average population in the bright state is above 0.5 due to the fluorescence branching ratios [Fig. 10 (inset)]. Upon application of a second ultrafast laser pulse, the coherence in the ion is maintained by driving the qubit states back down to the ground states (triangles).

in this excitation scheme is demonstrated using a microwave Ramsey experiment. In the absence of ultrafast laser pulses, the Ramsey contrast is essentially perfect. Following the application of the ultrafast laser pulse, the atom is driven to the excited state. The excited atom then spontaneously decays, and without precise measurement of the photon polarization, frequency, and emission time (with respect to the 14 GHz frequency qubit separation) the coherence is lost, as seen in Fig. 6(e). The uncontrolled measurement of the photon results in tracing over the photon portion of the density matrix, and the resulting loss in contrast is consistent with prior ion–photon entanglement.

To show that the excitation pulse is indeed coherently driving the superposition to the excited state, the Ramsey coherence is recovered by driving the ion back down to the ground state before spontaneous emission occurs [Fig. 6(c)]. With a pair of picosecond laser pulses incident on the ion between the microwave pulses, the contrast reappears with a phase shift proportional to the time Δt spent in the excited state and the hyperfine frequency difference between the ground and excited state levels: $\Delta t(\nu_0 - \nu_1) = (680\ \text{ps})(13.9\ \text{GHz}) = 18.9\pi$ [Fig. 6(e)]. The observed contrast is only 40% of the contrast without ultrafast laser pulses due to limited laser power in the second pulse and spontaneous decay ($\sim$23%) during the delay time between the ultrafast pulses.

7. REMOTE ATOM ENTANGLEMENT EXPERIMENTAL PROGRESS

A. Two-Photon Interference

Once two atoms are entangled with their respective photons, the next step for remote atom entanglement is the interference of the photon modes from each atom on a BS. Progress toward this end has been recently demonstrated.[81,82] In the cadmium ion system, two ions are placed in a trap and a BS setup is used to interfere the emitted photons (Fig. 7). In this setup, light scattered by the two ions is collected using an $f/2.1$ objective lens with a working distance of 13 mm. A pinhole is placed at the intermediate image for suppression of background photons and the intermediate image is reimaged by a doublet lens. The image is then broken up into two paths by a BS, and the transmitted and reflected beam pairs are directed to a second BS where the light from each ion is superimposed. Irises are used to block the unwanted beams,

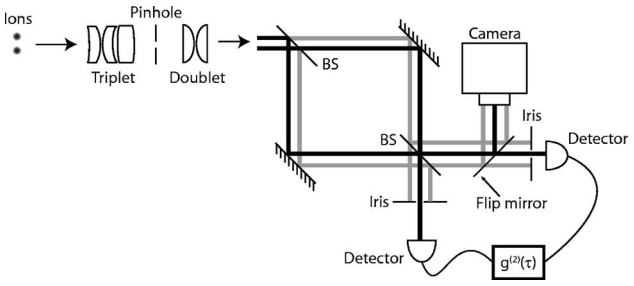

Fig. 7. Detection system for the two-photon interference experiment. The light from the two ions is separated on a BS and mode matched on the second BS. The photons are detected on single-photon sensitive PMTs. A camera is used for coarse alignment, and the nonoverlapping photon modes are blocked by irises.

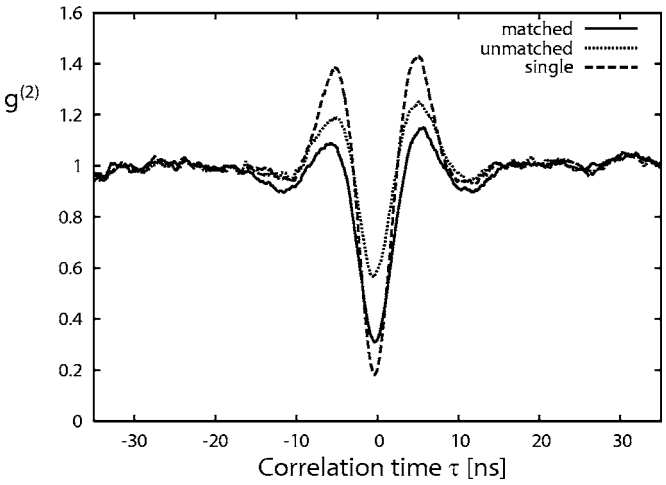

Fig. 8. Intensity autocorrelation for cw excitation. The dashed curve shows strong antibunching for a single ion with $g_1^{(2)}(0) = 0.18$ limited by the resolution of the detection system. With this value, the expected antibunching of light from two nonoverlapping ions is expected to be $g_{2,um}^{(2)}(0) = 0.59$ in good agreement with the experimental value (dotted curve). If the two-photon modes are matched, the interference leads to a significant reduction of coincidence detections (solid curve). The measured antibunching was $g_{2,m}^{(2)}(0) = 0.31$ corresponding to a mode overlap of $\sim$57%.

and the overlapping beams are directed to PMTs with a time resolution of $\sim$1 ns.[78] The equal path lengths of the transmitted and reflected beams ensure that the photons emitted by two ions are mode matched in size and divergence. Coarse alignment is performed by imaging the light after the second BS on a single-photon sensitive camera, where the overall magnification of the imaging system is $\sim$1000, and the diffraction-limited images of the two ions are separated by 2 mm, each with a spot size of 0.5 mm.

To demonstrate two-photon interference, first, the photon statistics of a single ion excited by a σ^+-polarized cw laser is investigated (dashed curve in Fig. 8). In this case, the $g^{(2)}$ autocorrelation function shows the expected damped Rabi oscillations[83,84] between the $^2S_{1/2}\ |1,1\rangle$ and $^2S_{3/2}\ |2,2\rangle$ levels. It is unlikely that two photons are emitted from one ion in close proximity, since after emission of a single photon, the ion is assured to be in the ground state. The maximum observed antibunching for the single ion is $g_1^{(2)}(0) = 0.18$ as expected for the time resolution of the PMTs.[82]

Next, two ions are equally illuminated and purposefully not mode matched on the BS. In this case, half of the signal results from two photons from the same ion, and the other half results from one photon from each ion. Since these photon modes are not matched on the BS, the detected photons are uncorrelated. We therefore expect a reduced antibunching, $g_{2,um}^{(2)}(0) = \frac{1}{2}[1 + g_1^{(2)}(0)] \approx 0.59$, in agreement with the measurement [dotted curve in Fig. 8].

If the photon modes from each ion are matched on the BS, then the photons always leave on the same output port, and thus no coincident detections are observed.[85] The suppression of coincidence events is clearly visible in the autocorrelation signal of the mode-matched ions (solid curve in Fig. 8) and has a measured $g_{2,m}^{(2)}(0)$ of 0.31. This corresponds to an interference signal of $\sim$57% (amplitude

matching of 75%) and compares well to the results observed in Ref. 81. This mode overlap is not ideal and is likely due to phase front distortions from the two atomic sources as they sample different parts of many optical surfaces before finally interfering on the BS.

To entangle two remotely located atoms, it is likely necessary to use single-mode optical fibers. This is because interfering the two photon modes requires very high stability of the atom and collection optics with respect to the BS, as well as good spatial mode matching from the two imaging systems. With free-space mode matching, any relative motion of the trapped atoms and the imaging optics can ruin the entanglement fidelity by producing false positive detection events, while in the fiber coupled case, effects such as mechanical vibrations and thermal drifts will simply lower the rate of coincidence counts (ignoring dark counts). In the cadmium system, however, the spontaneously emitted photons are deep in the ultraviolet at 214.5 nm, where it is very difficult to use optical fibers.

B. Single-Photon Sources

It is important for the atoms to emit only a single photon during an entanglement trial especially with remote-atom entanglement. Such a single-photon source was recently demonstrated in our laboratory by optically exciting a single cadmium ion using a picosecond mode-locked Ti:sapphire laser.[82] This laser is tuned to 858 nm and is sent through a pulse picker to reduce the repetition rate from 81 to 27 MHz with an extinction ratio of better than 100:1 in the infrared. The pulses are frequency quadrupled through single-pass nonlinear crystals, and the resulting 214.5 nm laser pulses have a pulse extinction ratio near 10^{-8} and a transform-limited pulse width of $\sim$1 ps. This allows for the excitation of the ion on a time scale much faster than the 2.65 ns excited state lifetime.

The single ion is repeatedly excited with the pulsed laser resulting in a periodic emission of photons at the laser pulse separation time of 37.5 ns, and the intensity autocorrelation function of the photons is recorded using a multichannel scaler (Fig. 9). The half-width of each peak is given by the excited state lifetime, and the peak at zero time delay corresponding to coincidentally detected photons is almost entirely suppressed. This near-perfect antibunching is highly nonclassical and demonstrates that at most one photon is emitted from the ion following an excitation pulse (limited by the possibility of emitting and detecting a photon *during* the excitation pulse $\approx 10^{-6}$). The residual peak at zero time delay has a height of $\sim$2% of the other peaks, originating from diffuse scattered light from the pulsed laser. With fast electronics, this residual peak could be identically zero by vetoing photons emitted during the picosecond laser pulse.

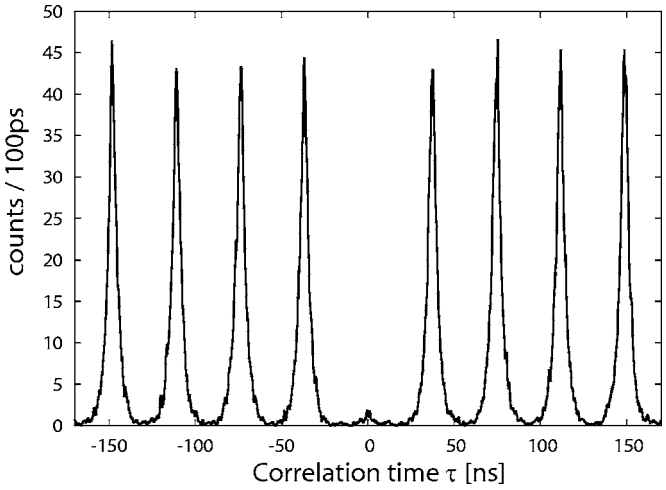

Fig. 9. Intensity autocorrelation of the light emitted by a single ion excited by an ultrafast laser. The near-perfect antibunching at $t=0$ shows that at most one photon is emitted from an excitation pulse.

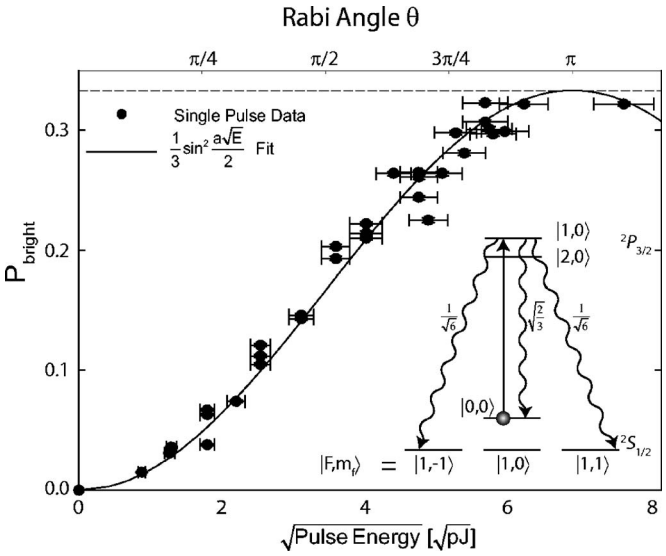

Fig. 10. Ion bright state population as a function of pulse energy. Each point represents a collection of 60,000 runs. As the population in the excited P state is driven to unity, the bright state population approaches 1/3 (horizontal dashed line) determined by the spontaneous emission branching ratio. The data are fit to a single parameter giving a value $a=0.42$ pJ$^{-1/2}$. Inset: Relevant energy levels for the $S-P$ Rabi oscillation experiment. A π-polarized ultrafast laser pulse excited the ion from the ground state to the excited state with variable energy. The three possible decay channels are shown with their respective fluorescence branching ratios. After a time (10 μs) following the excitation pulse, the bright state population of the ion was measured using resonance fluorescence detection.

The use of ultrafast lasers also allows for unit-probability excitation ($p_e \sim 1$) while maintaining a single-photon source. This corresponds to performing a Rabi π pulse on the optical $S-P$ transition. We observe optical Rabi flopping by measuring the Rabi angle as a function of pulse energy.

In the experiment, the Rabi angle is measured by preparing the ion in a known initial ground state and applying a single excitation pulse of known polarization.[49] With knowledge of the fluorescence branching ratios and the ability to perform efficient state detection, Rabi flopping with the pulsed laser can be detected using every laser pulse with a high signal-to-noise ratio (Fig. 10). An alternative method would be to detect the photon scattering rate from an ion as a function of the pulse energy, where Rabi angles with an odd (even) multiple of π would have a maximum (minimum) of scattered photons as the ion would be left in the excited (ground) state at the end of each pulse.[86]

In the experiment, the ion is prepared in the $|0,0\rangle$ ground state through optical pumping.[87] A single linearly polarized picosecond laser pulse excites the ion on the $P_{3/2}$ $|1,0\rangle$ state. After a time (10 μs), much longer than the excited state lifetime, the ion has decayed back to the $S_{1/2}$ ground-state levels via spontaneous emission following the fluorescence branching ratios. The atomic ground states are then measured using resonance fluorescence detection, where all three $F=1$ states are equally bright, while the $F=0$ state is dark[79,80,88] with the results shown in Fig. 10. The available power from the pulsed laser limits the Rabi rotation angle to roughly π, and the data agree well with the estimates based on the beam waist, pulse length, and pulse shape.[49] The probability of measuring the bright state is equal to 1/3 the probability of excitation to the excited state as follows from the CG coefficients [Fig. 10 (inset)]. Hence, we have shown that unit excitation and single-photon emission can be achieved with ultrafast laser pulses.

8. SCALING TO COMPLEX QUANTUM NETWORKS

A. Deterministic Quantum Computation and Quantum Repeaters

As the number of atoms grows within a trap used for a quantum register, so too does the complexity of the system. While there is progress in constructing more elaborate atom traps capable of deterministically separating and shuttling atoms,[23–26] an alternative approach is to keep traps relatively simple and have the atoms remain in a given trapping zone, where the necessary atomic motional control is relaxed. This approach requires the ability to interconnect different zones via photon-mediated entanglement (Fig. 11).

Recent progress has shown that remote deterministic quantum gates can be constructed for remotely located atoms even with the use of probabilistic entanglement.[90] Even though the entanglement is probabilistic, it is heralded, and one can simply repeat the procedure until the detectors announce the creation of the entangled pair of atoms. Once successful, the entanglement shared by the two atoms can be further used with local deterministic gates within each trapping zone.

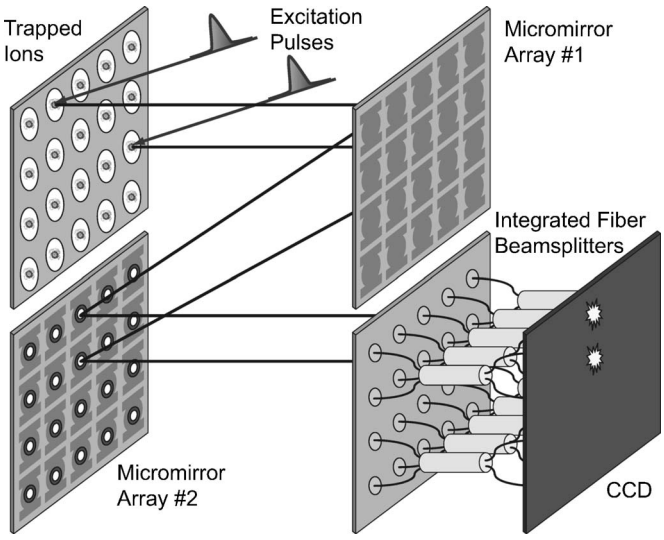

Fig. 11. Entanglement device capable of entangling multiple atoms simultaneously using micromirror arrays (Ref. 89). Any pair of atoms can be entangled by routing the emitted photon from each atom to a BS, where single-photon detections can project the atoms into an entangled state. Parallelism is possible with this setup for N atoms with $2N$ mirrors and $N/2$ BS pairs.

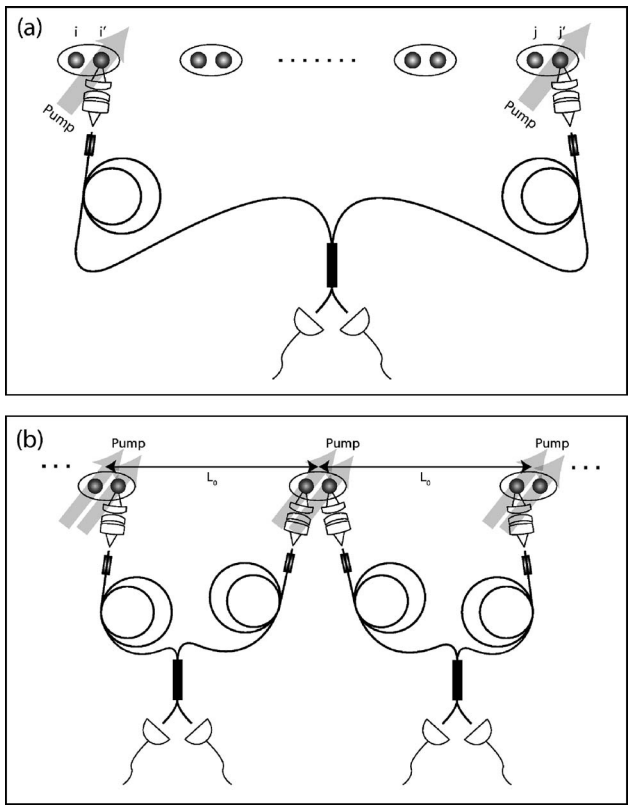

Fig. 12. (a) Schematic of the quantum computation model based on probabilistic photon-mediated entanglement between atoms. The ancilla atoms (i',j') are entangled through the probabilistic protocols described in the text, and deterministic gates on the logic atoms (i,j) are constructed from local motional gates and probabilistic remote ancilla entanglement. (b) Schematic of quantum repeaters with trapped atoms based on probabilistic remote entanglement and local Coulomb interactions.

One approach to scalable quantum computation based on probabilistic entangling gates is to have an array of trapping zones, each containing two atoms—a logic atom and an ancilla atom denoted as i and i', respectively [Fig. 12(a)].[90] The purpose of the logic atoms is to encode all quantum information, and the ancilla atoms, linked using the probabilistic entangling protocol, are used as a quantum bus. Once successful entanglement between the ancilla atoms is established, conventional local deterministic gates allow for an effective quantum gate between the two logic atoms. The resulting logic gate is deterministic, because the quantum information stored within the logic atoms is not affected by unsuccessful attempts to entangle the ancilla atoms. This can be assured by either spatial separation of the logic and ancilla atoms so that laser operations on one atom do not affect the other or by using different atomic species,[91–93] where the two atoms could be in very close proximity, since light resonant for operations on one atom would not affect the other.

There are four necessary steps to create deterministic remote atom entanglements: (1) attempt entanglement of the ancilla atoms until successful, (2) apply local deterministic motional controlled-NOT (CNOT) gates on each logic–ancilla pair, (3) measure the ancilla atoms in the appropriate bases, and (4) apply single-qubit rotations to the logic atoms based on the measurement results. The speed of each four-step procedure is limited by the first step. With a probability of successful entanglement P_{a-a} (of order $p^2p_e^2$), the average time for completion of the remote CNOT gate is T_{rep}/P_{a-a}, where as before, T_{rep} is the time needed for an ancilla entanglement trial.

Efficient quantum repeaters can also be constructed using this setup allowing for the reliable quantum information transfer over very long distances [Fig. 12(b)]. In addition to the entanglement probability mentioned previously, one must also consider the probability of photon loss within the fiber connecting the atomic nodes. This lowers the probability of successful ancilla atom entanglement to $P'_{a-a}=P_{a-a}P_{fiber}$, where $P_{fiber}=e^{-\alpha L_0}$ is the photon attenuation in the channel over the communication distance L_0, and α is the fiber attenuation coefficient. The time necessary to connect two nearest-neighbor segments (distance of L_0) would be $T_1=T_{rep}/P'_{a-a}$. This leads to a next-nearest-neighbor communication time of $T_2=2T_1$ and hence over n segments (total distance $D=nL_0$) of $T_n=nT_1=De^{\alpha L_0}(T_{rep}/P_{a-a})/L_0$. This linear scaling with distance compares favorably to the exponential scaling behavior if no repeater nodes are used: $T_n=e^{\alpha D}(T_{rep}/P_{a-a})$.

B. Cluster-State Model

Even though the above model for quantum computation is efficiently scalable with probabilistic entanglement between ancilla qubits, the robustness of the computation relies on the ability to perform local deterministic gates. Recent advances have shown that even if *all* entangling gates are probabilistic with arbitrarily small probability, one can still realize efficient quantum computation based on the use of deterministic single-bit operations and quantum memory.[28,29] The proof of this result is most convenient with the cluster-state approach to quantum computing. The cluster-state model is computationally equivalent to the conventional circuit model, but in terms of physical operations, it is quite different.[94] In this model, one first prepares a large-scale entangled state called the cluster state. Together with single-bit operations, the cluster state with a 2D geometry becomes sufficient for universal quantum computation.[94] As deterministic single-bit operations for trapped atoms has been demonstrated, the task then reduces to how to realize large-scale cluster states with only probabilistic entangling gates.

A pictorial description of the generation of cluster states with atomic qubits is shown in Fig. 13. The first step in creating a 2D cluster state is to generate long 1D cluster chains. One could start with entanglement of two atoms and then get these atoms further entangled with others one by one through the probabilistic gates. However, this direct approach leads to very inefficient (superexponential) scaling of the required resources due to the probabilistic nature of the gate operation.[29] For preparation of 1D cluster states, a way to overcome the inefficient

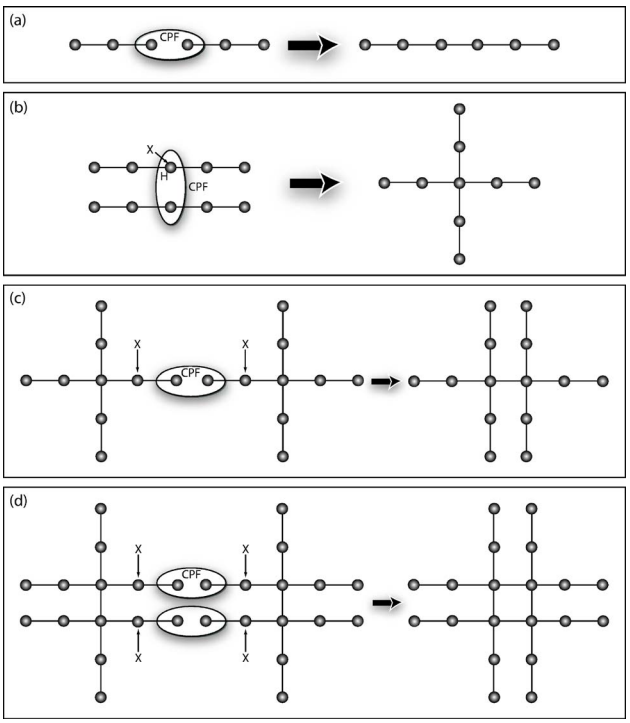

Fig. 13. Illustration of the necessary steps for the construction of cluster states. (a) Controlled phase flip (CPF) entangling gate is used to extend the length of a 1D cluster. (b) Construction of a cross-shaped cluster from two 1D cluster chains. A Hadamard gate (H) is applied on the middle qubit of one chain, and a CPF gate connects the two middle qubits. Finally, an X measurement on one middle qubit removes the extra atom. (c), (d) Construction of a square lattice cluster state from the cross-shaped cluster states. CPF gates combine the shapes along ends of the crosses and X measurements are used to remove the remaining redundant qubits.

scaling is through the divide-and-conquer protocol[28,29] (also known as the quantum repeater protocol in Ref. 95). With this approach, short 1D clusters of length n are created, and their end qubits are entangled through the probabilistic gate [Fig. 13(a)]. If the entanglement attempt between the end qubits is successful, then a 1D cluster of $2n$ qubits is made. If the attempt is unsuccessful, then only the end qubits and their nearest neighbors need to be removed from the cluster rather than the entire system losing its entanglement. The process is then repeated with the two clusters now each of a different length. Because this approach connects two cluster chains of almost equal lengths with the probabilistic gates, the number of connections grows logarithmically with the size of the chain, which is critical for efficient scaling.

Since 1D cluster states are not sufficient for universal computation, 2D clusters need to be built from the 1D chains. A straightforward extension of the divide-and-conquer method will not work as 2D and 1D geometries have very different characters,[28] in particular, for the number of the boundary qubits. To create 2D cluster states, these 1D clusters are first combined into a special type of state, called the cross state, as shown in [Fig. 13(b)], where 1D chains are first linked in their middles creating a cross-shaped cluster after a single-bit measurement. These cross states with four sufficiently long tails can be used as the basic building blocks for the 2D

geometry.[28] Once a cross is created, two such crosses are linked together via their long 1D tails. If the tail is sufficiently long, the two clusters can be connected almost deterministically before running out of qubits along the tail. Once connected, the remaining tail qubits separating the cross sections can be removed via single-bit X measurements finally creating the joined cluster [Fig. 13(c)]. These steps can be repeated to create a 2D cluster of any size. The fidelity of the cluster-state approach is not affected by the probabilistic nature of linking the atoms together, since the unsuccessful atoms are removed from the system. The scaling of the computational resources with this approach was demonstrated in Ref. 28. Supposing the success probability of the entangling gate is P_{a-a}, it has been proven there that the computational overhead to prepare a large-scale 2D cluster-state scales nearly polynominally with $1/P_{a-a}$ and n, where n is the total number of qubits in the cluster.

ACKNOWLEDGMENTS

This work is supported by the U.S. National Security Agency and the Disruptive Technology Office under Army Research Office contract W911NF-04-1-0234 and the National Science Foundation Information Technology Research Program.

D. L. Moehring's e-mail address is dmoehrin @umich.edu.

REFERENCES AND NOTES

1. C. Monroe, "Quantum information processing with atoms and photons," Nature **416**, 238–246 (2002).
2. J. Cirac and P. Zoller, "New frontiers in quantum information with atoms and ions," Phys. Today **57**, 38–45 (2004).
3. J. I. Cirac and P. Zoller, "Quantum computation with cold trapped ions," Phys. Rev. Lett. **74**, 4091–4094 (1995).
4. C. Monroe, D. M. Meekhof, B. E. King, W. M. Itano, and D. J. Wineland, "Demonstration of a fundamental quantum logic gate," Phys. Rev. Lett. **75**, 4714–4717 (1995).
5. A. Sørensen and K. Mølmer, "Quantum computation with ions in thermal motion," Phys. Rev. Lett. **82**, 1971–1975 (1999).
6. D. Jaksch, H.-J. Briegel, J. I. Cirac, C. W. Gardiner, and P. Zoller, "Entanglement of atoms via cold controlled collisions," Phys. Rev. Lett. **82**, 1975–1978 (1999).
7. D. Jaksch, J. I. Cirac, P. Zoller, S. L. Rolston, R. Côté, and M. D. Lukin, "Fast quantum gates for neutral atoms," Phys. Rev. Lett. **85**, 2208–2211 (2000).
8. C. A. Sackett, D. Kielpinski, B. E. King, C. Langer, V. Meyer, C. J. Myatt, M. Rowe, Q. A. Turchette, W. M. Itano, D. J. Wineland, and C. Monroe, "Experimental entanglement of four particles," Nature **404**, 256–259 (2000).
9. G. J. Milburn, S. Schneider, and D. F. V. James, "Ion trap quantum computing with warm ions," Fortschr. Phys. **48**, 801–810 (2000).
10. A. Sørensen and K. Mølmer, "Entanglement and quantum computation with ions in thermal motion," Phys. Rev. A **62**, 022311 (2000).
11. D. Jonathan, M. B. Plenio, and P. L. Knight, "Fast quantum gates for cold trapped ions," Phys. Rev. A **62**, 042307 (2000).
12. J. L. Cirac and P. Zoller, "A scalable quantum computer with ions in an array of microtraps," Nature **404**, 579–581 (2000).
13. C. J. Hood, T. W. Lynn, A. C. Doherty, A. S. Parkins, and H. J. Kimble, "The atom-cavity microscope: single atoms bound in orbit by single photons," Science **287**, 1447–1453 (2000).
14. P. W. H. Pinkse, T. Fischer, P. Maunz, and G. Rempe, "Trapping an atom with single photons," Nature **404**, 365–368 (2000).
15. L.-M. Duan, J. I. Cirac, and P. Zoller, "Geometric manipulation of trapped ions for quantum computation," Science **292**, 1695–1697 (2000).
16. I. H. Deutsch, G. K. Brennen, and P. S. Jessen, "Quantum computing with neutral atoms in an optical lattice," Fortschr. Phys. **48**, 925–943 (2000).
17. G. R. Guthöhrlein, M. Keller, K. Hayasaka, W. Lange, and H. Walther, "A single ion as a nanoscopic probe of an optical field," Nature **414**, 49–51 (2001).
18. D. Leibfried, B. DeMarco, V. Meyer, D. Lucas, M. Barrett, J. Britton, W. M. Itano, B. Jelenkovi, C. Langer, T. Rosenband, and D. J. Wineland, "Experimental demonstration of a robust, high-fidelity geometric two ion-qubit phase gate," Nature **422**, 412–415 (2003).
19. J. J. García-Ripoll, P. Zoller, and J. I. Cirac, "Speed optimized two-qubit gates with laser coherent control techniques for ion trap quantum computing," Phys. Rev. Lett. **91**, 157901 (2003).
20. F. Schmidt-Kaler, H. Häffner, M. Riebe, S. Gulde, G. P. T. Lancaster, T. Deuschle, C. Becher, C. F. Roos, J. Eschner, and R. Blatt, "Realization of the Cirac–Zoller controlled-NOT quantum gate," Nature **422**, 408–411 (2003).
21. L.-M. Duan, "Scaling ion trap quantum computation through fast quantum gates," Phys. Rev. Lett. **93**, 100502 (2004).
22. J. McKeever, A. Boca, A. D. Boozer, R. Miller, J. R. Buck, A. Kuzmich, and H. J. Kimble, "Deterministic generation of single photons from one atom trapped in a cavity," Science **303**, 1992–1994 (2004).
23. D. Kielpinski, C. Monroe, and D. Wineland, "Architecture for a large-scale ion-trap quantum computer," Nature **417**, 709–711 (2002).
24. M. A. Rowe, A. Ben-Kish, B. DeMarco, D. Leibfried, V. Meyer, J. Beall, J. Britton, J. Hughes, W. M. Itano, B. Jelenković, C. Langer, T. Rosenband, and D. J. Wineland, "Transport of quantum states and separation of ions in a dual rf ion trap," Quantum Inf. Comput. **2**, 257–271 (2002).
25. W. K. Hensinger, S. Olmschenk, D. Stick, D. Hucul, M. Yeo, M. Acton, L. Deslauriers, C. Monroe, and J. Rabchuk, "T-junction ion trap array for two-dimensional ion shuttling, storage and manipulation," Appl. Phys. Lett. **88**, 034101 (2006).
26. D. Stick, W. K. Hensinger, S. Olmschenk, M. J. Madsen, K. Schwab, and C. Monroe, "Ion trap in a semiconductor chip," Nat. Phys. **2**, 36–39 (2006).
27. L. Deslauriers, S. Olmschenk, D. Stick, W. K. Hensinger, J. Sterk, and C. Monroe, "Scaling and suppression of anomalous heating in ion traps," Phys. Rev. Lett. **97**, 103007 (2006).
28. L.-M. Duan and R. Raussendorf, "Efficient quantum computation with probabilistic quantum gates," Phys. Rev. Lett. **95**, 080503 (2005).
29. S. D. Barrett and P. Kok, "Efficient high-fidelity quantum computation using matter qubits and linear optics," Phys. Rev. A **71**, 060310(R) (2005).
30. L.-M. Duan, M. J. Madsen, D. L. Moehring, P. Maunz, R. N. Kohn, Jr., and C. Monroe, "Probabilistic quantum gates between remote atoms through interference of optical frequency qubits," Phys. Rev. A **73**, 062324 (2006).
31. J. I. Cirac, P. Zoller, H. J. Kimble, and H. Mabuchi, "Quantum state transfer and entanglement distribution among distant nodes in a quantum network," Phys. Rev. Lett. **78**, 3221–3224 (1997).
32. J. J. Bollinger, D. J. Heinzen, W. M. Itano, S. L. Gilbert, and D. J. Wineland, "A 303 MHz frequency standard based on trapped Be^+ ions," IEEE Trans. Instrum. Meas. **40**, 126–128 (1991).
33. C. Langer, R. Ozeri, J. D. Jost, J. Chiaverini, B. DeMarco, A. Ben-Kish, R. B. Blakestad, J. Britton, D. B. Hume, W. M. Itano, D. Leibfried, R. Reichle, T. Rosenband, T. Schaetz, P.

O. Schmidt, and D. J. Wineland, "Long-lived qubit memory using atomic ions," Phys. Rev. Lett. **95**, 060502 (2005).
34. H. Häffner, F. Schmidt-Kaler, W. Hänsel, C. F. Roos, T. Körber, M. Chwalla, M. Riebe, J. Benhelm, U. D. Rapol, C. Becher, and R. Blatt, "Robust entanglement," Appl. Phys. B **81**, 151–153 (2005).
35. A. Imamoglu, "Quantum computation using quantum dot spins and microcavities," Fortschr. Phys. **48**, 987–997 (2000).
36. C. Piermarocchi, P. Chen, L. J. Sham, and D. G. Steel, "Optical RKKY interaction between charged semiconductor quantum dots," Phys. Rev. Lett. **89**, 167402 (2002).
37. F. Troiani, E. Molinari, and U. Hohenester, "High-finesse optical quantum gates for electron spins in artificial molecules," Phys. Rev. Lett. **90**, 206802 (2003).
38. E. Pazy, E. Biolatti, T. Calarco, I. D'Amico, P. Zanardi, F. Rossi, and P. Zoller, "Spin-based optical quantum computation via Pauli blocking in semiconductor quantum dots," Europhys. Lett. **62**, 175–181 (2003).
39. T. Calarco, A. Datta, P. Fedichev, E. Pazy, and P. Zoller, "Spin-based all-optical quantum computation with quantum dots: understanding and suppressing decoherence," Phys. Rev. A **68**, 012310 (2003).
40. B. B. Blinov, D. Leibfried, C. Monroe, and D. J. Wineland, "Quantum computing with trapped ion hyperfine qubits," Quantum Inf. Process. **3**, 45–59 (2004).
41. D. Stucki, N. Gisin, O. Guinnard, G. Ribordy, and H. Zbinden, "Quantum key distribution over 67 km with a plug & play system," New J. Phys. **4**, 41 (2002).
42. D. S. Bethune and W. P. Risk, "Autocompensating quantum cryptography," New J. Phys. **4**, 42 (2002).
43. R. J. Hughes, J. E. Nordholt, D. Derkacs, and C. G. Peterson, "Practical free-space quantum key distribution over 10 km in daylight and at night," New J. Phys. **4**, 43 (2002).
44. N. Lütkenhaus and M. Jahma, "Quantum key distribution with realistic states: photon-number statistics in the photon-number splitting attack," New J. Phys. **4**, 44 (2002).
45. D. G. Enzer, P. G. Hadley, R. J. Hughes, C. G. Peterson, and P. G. Kwiat, "Entangled-photon six-state quantum cryptography," New J. Phys. **4**, 45 (2002).
46. C. Elliott, "Building the quantum network," New J. Phys. **4**, 46 (2002).
47. J. H. Shapiro, "Architectures for long-distance quantum teleportation," New J. Phys. **4**, 47 (2002).
48. It is also possible to excite on the D2 line to the $^2P_{3/2}$ manifold (for $I=1/2$) where the $|\uparrow\rangle$ and $|\downarrow\rangle$ states are excited to $|F'=1, m_{F'}=0\rangle$ and $|F'=2, m_{F'}=0\rangle$, respectively.
49. M. J. Madsen, D. L. Moehring, P. Maunz, R. N. Kohn, Jr., L.-M. Duan, and C. Monroe, "Ultrafast coherent coupling of atomic hyperfine and photon frequency qubits," Phys. Rev. Lett. **97**, 040505 (2006).
50. A. Mundt, A. Kreuter, C. Becher, D. Leibfried, J. Eschner, F. Schmidt-Kaler, and R. Blatt, "Coupling a single atomic quantum bit to a high finesse optical cavity," Phys. Rev. Lett. **89**, 103001 (2002).
51. A. Kuhn, M. Hennrich, and G. Rempe, "Deterministic single-photon source for distributed quantum networking," Phys. Rev. Lett. **89**, 067901 (2002).
52. P. G. Kwiat, A. M. Steinberg, R. Y. Chiao, P. Eberhard, and M. Petroff, "High efficiency single-photon detectors," Phys. Rev. A **48**, R867–R870 (1993).
53. A. P. VanDevender and P. G. Kwiat, "High efficiency single photon detection via frequency up-conversion," J. Mod. Opt. **51**, 1433–1445 (2004).
54. D. Rosenberg, A. E. Lita, A. J. Miller, and S. W. Nam, "Noise-free high-efficiency photon-number-resolving detectors," Phys. Rev. A **71**, 061803 (2005).
55. C. Cabrillo, J. I. Cirac, P. Garcia-Fernandez, and P. Zoller, "Creation of entangled states of distant atoms by interference," Phys. Rev. A **59**, 1025–1033 (1999).
56. L.-M. Duan and J. Kimble, "Efficient engineering of multiatom entanglement through single-photon detections," Phys. Rev. Lett. **90**, 253601 (2003).
57. C. Simon and W. T. M. Irvine, "Robust long-distance entanglement and a loophole-free Bell test with ions and photons," Phys. Rev. Lett. **91**, 110405 (2003).
58. U. Eichmann, J. C. Bergquist, J. J. Bollinger, J. M. Gilligan, W. M. Itano, D. J. Wineland, and M. G. Raizen, "Young's interference experiment with light scattered from two atoms," Phys. Rev. Lett. **70**, 2359–2362 (1993).
59. W. M. Itano, J. C. Bergquist, J. J. Bollinger, D. J. Wineland, U. Eichmann, and M. G. Raizen, "Complementarity and Young's interference fringes from two atoms," Phys. Rev. A **57**, 4176–4187 (1998).
60. C. K. Hong, Z. Y. Ou, and L. Mandel, "Measurement of subpicosecond time intervals between two photons by interference," Phys. Rev. Lett. **59**, 2044–2046 (1987).
61. B. Yurke, S. L. McCall, and J. R. Klauder, "SU(2) and SU(1,1) interferometers," Phys. Rev. A **33**, 4033–4054 (1986).
62. A. R. Edmunds, *Angular Momentum in Quantum Mechanics* (Princeton U. Press, 1960).
63. S. J. Freedman and J. F. Clauser, "Experimental test of local hidden-variable theories," Phys. Rev. Lett. **28**, 938–941 (1972).
64. A. Aspect, P. Grangier, and G. Roger, "Experimental realization of Einstein-Podolsky-Rosen-Bohm *gedankenexperiment*: a new violation of Bell's inequalities," Phys. Rev. Lett. **49**, 91–94 (1982).
65. R. G. DeVoe and R. G. Brewer, "Observation of superradiant and subradiant spontaneous emission of two trapped ions," Phys. Rev. Lett. **76**, 2049–2052 (1996).
66. A. Kuzmich, L. Mandel, and N. P. Bigelow, "Generation of spin squeezing via continuous quantum nondemolition measurement," Phys. Rev. Lett. **85**, 1594–1597 (2000).
67. B. Julsgaard, A. Kozhekin, and E. S. Polzik, "Experimental long-lived entanglement of two macroscopic objects," Nature **413**, 400–403 (2001).
68. S. Haroche, J. M. Raimond, and M. Brune, *Experimental Quantum Computation and Information* (IOS Press, 2002), pp. 3–36.
69. A. Kuhn and G. Rempe, *Experimental Quantum Computation and Information* (IOS Press, 2002), pp. 37–66.
70. A. Kuzmich, W. P. Bowen, A. D. Boozer, A. Boca, C. W. Chou, L.-M. Duan, and H. J. Kimble, "Generation of nonclassical photon pairs for scalable quantum communication with atomic ensembles," Nature **423**, 731–734 (2003).
71. C. H. van der Wal, M. D. Eisaman, A. Andr, R. L. Walsworth, D. F. Phillips, A. S. Zibrov, and M. D. Lukin, "Atomic memory for correlated photon states," Science **301**, 196–200 (2003).
72. J. McKeever, J. R. Buck, A. D. Boozer, A. Kuzmich, H.-C. Nägerl, D. M. Stamper-Kurn, and H. J. Kimble, "State-insensitive cooling and trapping of single atoms in an optical cavity," Phys. Rev. Lett. **90**, 133602 (2003).
73. B. B. Blinov, D. L. Moehring, L.-M. Duan, and C. Monroe, "Observation of entanglement between a single trapped atom and a single photon," Nature **428**, 153–157 (2004).
74. D. L. Moehring, M. J. Madsen, B. B. Blinov, and C. Monroe, "Experimental Bell inequality violation with an atom and a photon," Phys. Rev. Lett. **93**, 090410 (2004).
75. D. N. Matsukevich and A. Kuzmich, "Quantum state transfer between matter and light," Science **306**, 663–666 (2004).
76. C. W. Chou, H. de Riedmatten, D. Felinto, S. V. Polyakov, S. J. van Enk, and H. J. Kimble, "Measurement-induced entanglement for excitation stored in remote atomic ensembles," Nature **438**, 828–832 (2005).
77. J. Volz, M. Weber, D. Schlenk, W. Rosenfeld, J. Vrana, K. Saucke, C. Kurtsiefer, and H. Weinfurter, "Observation of entanglement of a single photon with a trapped atom," Phys. Rev. Lett. **96**, 030404 (2006).
78. D. L. Moehring, B. B. Blinov, D. W. Gidley, R. N. Kohn, Jr., M. J. Madsen, T. B. Sanderson, R. S. Vallery, and C. Monroe, "Precision lifetime measurement of a single trapped ion with ultrafast laser pulses," Phys. Rev. A **73**, 023413 (2006).

79. R. Blatt and P. Zoller, "Quantum jumps in atomic systems," Eur. J. Phys. **9**, 250–256 (1988).
80. M. Acton, K.-A. Brickman, P. Haljan, P. J. Lee, L. Deslauriers, and C. Monroe, "Near-perfect simultaneous measurement of a qubit register," Quantum Inf. Comput. **6**, 465–482 (2006).
81. J. Beugnon, M. P. A. Jones, J. Dingjan, B. Darquie, G. Messin, A. Browaeys, and P. Grangier, "Quantum interference between two single photons emitted by independently trapped atoms," Nature **440**, 779–782 (2006).
82. P. Maunz, M. J. Madsen, D. L. Moehring, R. N. Kohn, Jr., K. Younge, and C. Monroe, "Quantum interference of photon pairs from two trapped atomic ions," arXiv.org e-Print archive, August 5, 2006, quant-ph/0608047, http://arXiv.org/labs/quant-ph/0608047.
83. F. Diedrich and H. Walther, "Nonclassical radiation of a single stored ion," Phys. Rev. Lett. **58**, 203–206 (1987).
84. W. M. Itano, J. C. Bergquist, and D. J. Wineland, "Photon antibunching and sub-Poissonian statistics from quantum jumps in one and two atoms," Phys. Rev. A **38**, 559–562 (1988).
85. L. Mandel, "Quantum effects in one-photon and two-photon interference," Rev. Mod. Phys. **71**, S274–S282 (1999).
86. B. Darquie, M. P. A. Jones, J. Dingjan, J. Beugnon, S. Bergamini, Y. Sortais, G. Messin, A. Browaeys, and P. Grangier, "Controlled single-photon emission from a single trapped two-level atom," Science **309**, 454–456 (2005).
87. P. J. Lee, B. B. Blinov, K. Brickman, L. Deslauriers, M. J. Madsen, R. Miller, D. L. Moehring, D. Stick, and C. Monroe, "Atomic qubit manipulations with an electro-optic modulator," Opt. Lett. **28**, 1582–1584 (2003).
88. P. J. Lee, K.-A. Brickman, L. Deslauriers, P. C. Haljan, L.-M. Duan, and C. Monroe, "Phase control of trapped ion quantum gates," J. Opt. B: Quantum Semiclassical Opt. **7**, S371–S383 (2005).
89. J. Kim, C. J. Nuzman, B. Kumar, D. F. Lieuwen, J. S. Kraus, A. Weiss, C. P. Lichtenwalner, A. R. Papazian, R. E. Frahm, N. R. Basavanhally, D. A. Ramsey, V. A. Aksyuk, F. Pardo, M. E. Simon, V. Lifton, H. B. Chan, M. Haueis, A. Gasparyan, H. R. Shea, S. Arney, C. A. Bolle, P. R. Kolodner, R. Ryf, D. T. Neilson, and J. V. Gates, "1100 $\times$1100 port MEMS-based optical crossconnect with 4-dB maximum loss," IEEE Photon. Technol. Lett. **15**, 1537–1539 (2003).
90. L.-M. Duan, B. B. Blinov, D. L. Moehring, and C. Monroe, "Scaling trapped ions for quantum computation with probabilistic ion-photon mapping," Quantum Inf. Comput. **4**, 165–173 (2004).
91. B. B. Blinov, L. Deslauriers, P. Lee, M. J. Madsen, R. Miller, and C. Monroe, "Sympathetic cooling of trapped Cd^+ isotopes," Phys. Rev. A **65**, 040304(R) (2002).
92. M. Barrett, B. L. DeMarco, T. Schaetz, V. Meyer, D. Leibfried, J. Britton, J. Chiaverini, W. M. Itano, B. M. Jelenkovic, J. D. Jost, C. Langer, T. Rosenband, and D. J. Wineland, "Sympathetic cooling of $^9Be^+$ and $^{24}Mg^+$ for quantum logic," Phys. Rev. A **68**, 042302 (2003).
93. P. O. Schmidt, T. Rosenband, C. Langer, W. M. Itano, J. C. Bergquist, and D. J. Wineland, "Spectroscopy using quantum logic," Science **309**, 749–752 (2005).
94. R. Raussendorf and H. J. Briegel, "A one-way quantum computer," Phys. Rev. Lett. **86**, 5188–5191 (2001).
95. L.-M. Duan, M. D. Lukin, J. I. Cirac, and P. Zoller, "Long-distance quantum communication with atomic ensembles and linear optics," Nature **414**, 413–418 (2001).